WILEY-VCH

DOI: 10.1002/ ((please add manuscript number))

Article type: Review

Degradability and Clearance of Inorganic Nanoparticles for Biomedical Applications

*Guangbao Yang, Soo Zeng Fiona Phua, Anivind Kaur Bindra, Yanli Zhao**

Dr. G. Yang, S. Z. F. Phua, A. K. Bindra, Prof. Y. L. Zhao

Division of Chemistry and Biological Chemistry, School of Physical and Mathematical Sciences, Nanyang Technological University, 21 Nanyang Link, 637371, Singapore

Prof. Y. L. Zhao

School of Materials Science and Engineering, Nanyang Technological University, 50 Nanyang Avenue, 639798, Singapore

*E-mail: zhaoyanli@ntu.edu.sg

Abstract

Inorganic nanoparticles with tunable and diverse properties hold a tremendous potential in the field of nanomedicine, while having non-negligible toxicity concerns in healthy tissues/organs that resulted in their restricted clinical translation to date. In the past decade, the emergence of biodegradable or clearable inorganic nanoparticles has made it possible to completely solve this long-standing conundrum. A comprehensive understanding on the design of these inorganic nanoparticles with their metabolic performance in the body is of crucial importance to advance clinical trials and expand their biological applications in disease diagnosis. In this review, we highlight a diverse variety of biodegradable or clearable inorganic

nanoparticles with regard to the considerations of size, morphology, surface chemistry and doping strategy. Their pharmacokinetics, pathways of metabolism in the body, and time required for excretion are discussed. Some inorganic materials intrinsically responsive to various conditions in the tumor microenvironment are also introduced. Finally, we provide an overview of the encountered challenges and an outlook for applying these inorganic nanoparticles toward future clinical translations.

Keywords: biomedicine, excretion, inorganic nanoparticles, metabolism, pharmacokinetics

1 Introduction

Nanotechnology has shown an immense potential in the diagnosis and treatment of diseases, and a large number of nanomaterials with different compositions and structures have been developed to overcome the drawbacks of traditional treatments.[1] These nanomaterials developed for nanomedicine could be classified into three main categories: (1) inorganic, (2) organic and (3) organic-inorganic hybrid nanosystems.[2] In particular, variable composition of inorganic nanoparticles possesses distinct physical and chemical properties as well as versatile morphologies and sizes, providing unprecedented opportunities for novel biomedical applications.[3] Thus, inorganic nanomaterials, including quantum dots (QDs),[4] carbon-based nanomaterials,[5] silica-based nanomaterials and metallic nanoparticles,[6] have been designed and applied for diagnosis and treatment of diseases. However, inorganic nanoparticles often accumulate largely in the reticuloendothelial system (RES) to result in low passive targeting specificity and long-term toxicity, thus hindering the advancements of such nanomaterials for clinical trials.[7]

The US Food and Drug Administration (FDA) requires all administrated contrast agents to be completely cleared from the body in a relatively short span of time.[8] Systematic evaluation on the toxicity and metabolic behavior of nanomaterials in the body is essential to impel their clinical transition and extend their applications in disease theranostics. The

clearance of nanoparticles follows two main pathways in metabolic processes: (1) urinary excretion and (2) hepatobiliary and feces excretion.[9] Nanoparticles with the sizes exceeding 6 nm or containing heavy metals could be rapidly taken up by the RES (liver and spleen). Nanoparticles with small sizes (< 5.5 nm) are quickly metabolized in the urine by the urinary system because their sizes fall below the threshold required for kidney filtration.[10] Some nanoparticles with large sizes could be cleared by kidney after their degradation during the prolonged circulation in the body.[11] Therefore, the development of rapidly cleared nanoparticles is an intricate task that needs to be adequately explored for biomedical applications, especially for the translation of such nanomaterials into clinical trials.

In order to greatly minimize the non-specific accumulation and potential long-term toxicity in the RES organs, several different kinds of biodegradable or clearable inorganic nanoparticles have been developed.[12] This review aims to summarize the recent developments on the biodegradation and specific metabolic pathways of some representative inorganic materials such as QDs with different compositions, multi-structured silica, and a wide variety of metal-containing inorganic compounds **(Figure 1)**. Through tuning their sizes and morphologies, surface chemistry and doping strategies, the designed inorganic nanoparticles can be rapidly decomposed under specific physiological conditions and then easily excreted by different metabolic pathways. Some of the inorganic nanoparticles with ultra-small sizes (< 5.5 nm) can also be rapidly metabolized by urinary system in a short period of time, while maintaining their morphology. We believe that this review would provide useful insights and understanding to the biomedical applications of inorganic nanomaterials for the promotion of their future clinical translation in the theranostics of diseases.

2 Quantum Dots

QDs with high quality have been explored by optimizing synthetic procedures, enhancing

quantum yields, and functionalizing with targeted molecules and therapeutic agents.[13] QDs generally contain the atoms of group Ⅱ-Ⅵ elements (e.g., CdS, CdSe, CdTe, ZnS and ZnSe),[14] group Ⅳ-Ⅵ elements (e.g., PbS, PbSe and PbTe),[15] group Ⅳ elements (e.g., C, Si and Ge)[16] and group Ⅵ elements (e.g., Mo and W).[17] They have been proven useful in biomedicine including sensing, imaging and enhanced treatment of diseases. Concurrently, several studies have been carried out pertaining to the potential clearance of QDs through the renal system after administration. In 2007, the pioneer work for renal clearance of QDs illustrated that a hydrodynamic size (HD) of ≤ 5.5 nm would induce fast urinary excretion and clearance of QDs.[8]

2.1 Carbon nanomaterial-based quantum dots

Carbon dots (CDs) serving as a new type of fluorescent probes can be easily functionalized to increase their solubility and lower the toxicity, in contrast with traditional semiconductor QDs.[18] It has been revealed that CDs meet several basic conditions for clinical applications: rapid excretion from the body, low toxicity, and ability to generate trusted optical signals. Thus, various types of CDs have been employed for phototherapy, used as contrast agents for imaging, and conjugated with therapeutic species for combination therapy.[19]

To date, many *in vivo* studies have been performed to understand the biodistribution of CDs. In 2009, Yang *et al.* presented the detailed study of CDs with various injection ways for optical imaging *in vivo* to reveal their nontoxic and biocompatible characteristics.[20] Subsequently, it has been reported that CDs with the size of ~ 3 nm were rapidly and efficiently excreted from the mouse body after different injection approaches: intravenous (i.v.), subcutaneous (s.c.) and intramuscular (i.m.) **(Figure 2a,b)**.[21] Specifically, the i.v. injection of CDs suggested much faster urine clearance than that of s.c. and i.m. injection routes, which showed the clearance rate of CDs as i.v. > i.m. > s.c. **(Figure 2c,d)**. This study also demonstrated that the injection route could influence the rate of blood and urine clearance, the

biodistribution in different organs, and the tumor accumulation of CDs. Moreover, different surface charges of CDs were also shown to be a key factor in their distribution after i.v. injection. For instance, Licciardello *et al.* reported that silicon nanoparticles and CDs with positively charged surface showed high uptake in the liver and intestine, probably owing to the production of a protein corona.[22] Conversely, neutral or zwitterionic particles with little hepatic uptake were rapidly cleared through the urinary bladder by renal excretion. Therefore, different hydrophilicity and surface charge of the nanoparticles may induce distinct performance in the biodistribution, clearable pathway and pharmacokinetic properties.

As promising carbon-based imaging probes, carbon nanodots (CNDs) have also attracted enough attention because of their excellent water solubility, biocompatibility and photostability.[23] Kim and coworkers developed nitrogen (N) doped CNDs (N-CNDs) with an ultrasmall particle size of ~3 nm, which could be used both as a photoacoustic (PA) contrast agent and a photothermal agent with strong absorption in the near-infrared (NIR) region **(Figure 3a-d)**.[24] Finally, the biodegradability and renal excretion of N-CNDs were verified by whole body PA imaging and degradation experiments **(Figure 3e,f)**.

As one of the most rapidly developed carbon nanomaterials, graphene quantum dots (GQDs) with very small lateral dimensions (< 10 nm) have been employed for biomedical applications, because of their strong fluorescence, high quantum yields, and inherent advantages of graphene.[25] The detailed distribution and clearance pathway of GQDs after administration have been examined by some researchers. For instance, Nurunnabi *et al.* developed carboxylated photoluminescent GQDs and examined their *in vivo* distribution and potential toxicity in mice, concluding that the GQDs would accumulate in major organs (such as liver, spleen, lung and kidney) of the animal models after i.v. injection.[26] The same research team also synthesized a series of polydopamine (PDA)-coated GQDs with the sizes ranging from 9 to 30 nm. After i.v. injection of different GQDs, relatively low fluorescence intensity of free GQDs without the PDA coating showed renal clearance when the sizes were in the range

of 3-6 nm at 4 h post injection.[27] In addition, Chong *et al.* reported that Cy7-labeled GQD-PEG (PEG = polyethylene glycol) mainly accumulated in kidney with minimal accumulation in other organs.[28] More importantly, strong Cy7 fluorescence was observed in tumor, demonstrating that PEG could enhance the accumulation of GQD-PEG with the help of enhanced permeability and retention (EPR) effect. These findings may accelerate the research development of low toxic GQD-based bioimaging and drug delivery systems for efficient cancer therapy.

2.2 Silicon quantum dots

Silicon as an element possesses low toxicity and has sometimes been regarded as a semiconductor with low bandgap, which can be easily induced to exhibit significant changes in optical characteristics when its crystal width is reduced to less than approximately 4 nm. Based on these unique properties, silicon quantum dots (Si QDs) exhibit promising biomedical applications, having potential biodegradability to form non-toxic silicic acid that can be rapidly excreted through urine.[29]

In an early study by Louie and co-workers, the *in vivo* biodistribution of Si QDs radiolabeled with $^{64}Cu^{2+}$ complex was investigated using *in vivo* positron emission tomography (PET) imaging **(Figure 4a)**.[30] The results demonstrated that the dextran coated Si QDs were quickly metabolized from the blood stream and further excreted from the body through urinary system, while the Si QDs with larger HD accumulated in the liver **(Figure 4b)**. Different HD and diverse surface coating on Si QDs may induce different clearable pathways. For instance, May *et al.* presented that Pluronic® block copolymers could effectively encapsulate Si QDs, allowing them to achieve excellent dispersibility in water.[31] The presence of micellar layer encapsulating the Si QDs resulted in the formation of nanoparticles with diameters of 20-150 nm as observed by transmission electron microscopy (TEM). The *in vivo* fluorescence images exhibited that the micelle coated Si QDs did not accumulate in heart, lung and brain. They were found only in the RES (liver and spleen), where they were excreted into the biliary system and

finally entered the gall bladder and intestine.

2.3 Cadmium-based quantum dots

The majority of QD-related studies in biomedicine including imaging and sensing is Cd-based QDs such as CdS, CdSe, and CdTe/CdSe core/shell QDs, where ZnS or ZnSe is usually coated to serve as a protecting shell.[32] Researchers optimized reaction conditions by employing readily accessible precursors and simple liquid phase synthesis methods to synthesize Cd-based QDs for general bioimaging and therapeutic applications.

To evaluate the threshold for the renal filtration, Frangioni group reported DL-cystine coating on a CdSe/ZnCdS core/shell structure with an extraordinarily small size of ~ 6 nm, inducing renal clearance of Cd-based QDs in rat models.[33] Neutrally charged QDs of this size at normal physiological conditions did not aggregate and could accumulate in the bladder after 4 h post i.v. injection, suggesting that the size of DL-cystine coated QDs was near or below the renal clearance threshold. When increasing the size, the DL-cystine coated QDs showed no obvious renal clearance at 4 h post injection after incubated with fetal bovine serum (FBS) at different pH (6.0 and 9.0) for 4 h. These results indicated that the size of QDs was the major factor that renders the effectiveness of the renal clearance of QDs from the body.

The abovementioned strategies for modifying Cd-based QDs with new surface functionality usually involve the complexity in the synthetic procedures. Amorphous silica is a biocompatible material that can be utilized for coating the surface of QDs for biomedical applications. Rao and coworkers reported that the as-prepared silica coated CdTe QDs could hinder the release of QD components into the physiological environment and thus enhance the biocompatibility of QDs **(Figure 5a)**.[34] Furthermore, the silica-coated CdTe QDs showed more favorable renal clearance than commercially available QD605 with similar photophysical properties and size **(Figure 5b,c)**. In addition, their low uptake in liver and spleen and extended blood circulation were beneficial to biomedical applications **(Figure 5d,e)**.

3 Silica nanoparticles

Silica nanoparticles have been widely used for various applications, including bioimaging, cargo delivery and disease treatment.[35] Most of these applications were realized by adjusting the parameters such as size, morphology, surface properties and framework structure.[36] The biocompatibility and degradability of silica nanoparticles have been explored by several research groups *in vitro* and *in vivo*.[37] Studies have been carried out to evaluate the accumulation of the silica nanocarriers in order to avoid any side effects. Herein, the specific degradability and clearance of different silica nanoparticles are introduced.

3.1 Degradation and clearance trends

Various factors have been evaluated to understand the degradation and clearance trends of silica nanoparticles, which include size, morphology, surface functionalization and so on. The size of silica nanoparticles is related to the special properties they possess and may play a key role in toxicity research.[38] Kuroda and coworkers reported four different types of colloidal mesoporous silica nanoparticles (CMPS) with various particle sizes (ca. 20-80 nm), using tetraalkoxysilanes to regulate hydrolysis rates by one-pot method.[39] It was observed that about 15 % CMPS framework degraded per day, and more than 90 % of nanoparticles degraded after one week, regardless of the nanoparticle size. The similar rate of degradation for these four types of CMPS was a result of their similar surface areas. The Stöber method could be used to prepare uniform mesoporous silica nanoparticles (UMSNs), presenting different structures from those mesoporous silica nanoparticles (MSNs) synthesized in aqueous solution. Lu and coworkers prepared UMSNs with different sizes in a mixed solution of water and ethanol.[40] More than 95 % of these four different sized UMSNs (*i.e.*, 150 ± 20 nm, 200 ± 21 nm, 310 ± 15 nm and 390 ± 11 nm) degraded in simulated body fluid (SBF), showing similar degradation profiles. As compared with MSNs synthesized in aqueous phase, UMSNs could generate hollow structures and be better dispersed during the degradation process.

To facilitate the application of degradable materials in the biomedical field, the information on the distribution, metabolism and excretion of silica nanoparticles would be essential. He *et al.* investigated the *in vivo* biodistribution and excretion of MSNs with various sizes (80, 120, 200 and 360 nm) for up to 1 month, and the PEGylation effect was also discussed **(Figure 6a)**.[41] The PEGylation of MSNs could slightly alleviate the uptake of the nanoparticles by liver, spleen and lung, which thus prolonged the blood circulation half-life and resulted in lower biodegradation and excretion than bare MSNs with the same sizes. MSNs with smaller nanoparticle sizes could escape the capture by liver and spleen more easily, and slow down their degradation and excretion of degraded products **(Figure 6b)**.

It has been proven that the shape of nanoparticles could determine their *in vivo* kinetics, biodegradation and clearance.[42] Tang and coworkers designed different shaped fluorescent MSNs (aspect ratios: 1.5 and 5) by varying the concentrations of reaction reagents in order to study the impact of the shape and PEG modification on *in vivo* biocompatibility, distribution and excretion **(Figure 6c)**.[43] Short-rod MSNs tended to accumulate in the liver, while long-rod MSNs were trapped in the spleen. Interestingly, all MSNs showed high retention in the lung after they were modified with PEG. The data further exhibited that most of the MSNs were excreted through urine and feces, and their speed of clearance was mainly determined by the shape of MSNs, where long-rod MSNs had slower clearance rate than that of short-rod MSNs under metabolic routes **(Figure 6d)**. MCM-41 type MSNs with similar diameter, pore size and surface charge having varied aspect ratios (1, 2 and 4) were prepared, and the influence of nanoparticle shape on the degradation behavior was assessed by the same research team.[44] The conclusions were that spherical nanoparticles (with and without PEG modification) degraded more rapidly than short and long rod-shaped ones (with and without PEG modification), due to the difference in their exterior surface areas. In addition, the PEG modification obviously influenced the degradation rate and mode of MSNs. Due to steric hindrance of the hydrophilic PEG, the degradation of PEG functionalized MSNs started from the interior of nanoparticles,

whereas the naked MSNs degraded from their external surface.

The influence of the surface modification on silica nanomaterials was also investigated. To evaluate the substantial effect of different PEG chain lengths on the behavior of nanoparticles, Bein and coworkers designed colloidal core-shell mesoporous silica (CMS) with different types of linear PEG modifications (PEG lengths: M_w 550 and 5000 as well as their mixture).[45] The PEG shell could decrease the degradation rate of silica nanoparticles in SBF in comparison to the unfunctionalized ones. The main reason for the slow degradation could be ascribed to the presence of PEG shell on the surface of silica nanoparticles. PEG with the hydrophilicity could resist the adhesion and prevent the adsorption of proteins, thereby reducing undesired interactions between physiological environments and silica nanoparticles. Notably, the degradation rate of the silica nanoparticles that were functionalized with longer and denser PEG chains was found to be slower as compared to those nanoparticles functionalized with shorter PEG chains. Three types of surface-modified silica nanoparticles with the size of ~45 nm, termed as OH-SiNPs, COOH-SiNPs and PEG-SiNPs, were also studied by He *et al.* to evaluate their biodistribution and urinary excretion **(Figure 7a,b)**.[46] *In vivo* optical images from the bladder and urine excretion exhibited that all these nanoparticles could be partially cleared by the renal excretion route, showing the independence of such modifications on the renal clearance **(Figure 7c)**. On the other hand, the PEG-SiNPs revealed comparatively longer blood circulation and lower liver uptake as compared to that of OH-SiNPs and COOH-SiNPs.

Other surface functionalities could also impact the degradation rate of silica nanoparticles. Kim *et al.* explored the biodegradation of hexagonally ordered mesoporous silica, SBA-15, in SBF.[47] In order to study the effect of different surface functionalities on the degradation behavior, SBA-15 was functionally modified with hydroxyl (OH), amine (NH_2) and carboxylic (COOH) moieties on the surface. The COOH-SBA-15 presented the lowest degradation percentage of 70.7 %, while OH-SBA-15 and NH_2-SBA-15 showed 91.5 % and 86.6 % degradation, respectively. These studies indicate that different kinds of surface modifications

on SBA-15 could induce slower degradation rate than that of pristine SBA-15, meaning that functional groups could interfere with the corrosion of silica shell by interacting with cations in SBF to reduce the degradation rate of SBA-15. Vallet-Regí and coworkers also verified that the degradation rate of SBA-15 could be reduced by organically modifying with different organic groups, *i.e.*, alkyl chains (methyl and octyl) and amino propyl groups, as compared to unmodified SBA-15, attributed by the organic species coverage acting as a protection barrier.[48]

Apart from the abovementioned factors, some parameters including pore size, surface area and charge also have an important impact on the biodegradation and excretion of silica nanoparticles.[49] For example, He *et al.* studied the effect of surface area and initial concentration of MSNs on their three stages of degradation.[50] The results demonstrated that both high concentrations and low surface areas would lower the percentage of degradation, thus raising the degradation time. Nanoparticles with either positive or negative surface charges may have the interaction with the serum proteins, which would further influence their biodistribution. Therefore, it is of primary importance to investigate the impact of charges on the biodegradation and excretion of nanoparticles. Souris *et al.* reported that near-infrared fluorescent MSNs with highly positive charge showed the most rapid hepatobiliary excretion.[51] MSNs were conjugated with an indocyanine green dye through covalent or ionic bonding to obtain particles with similar structures but different surface charges. It was found that the highly charged particles (+34.4 mV at pH 7.4) could be easily cleared from stomach and intestines, while particles that were negatively charged (-17.6 mV at physiological pH) remained in the liver. These data exhibited that the adsorption of serum proteins was charge-dependent, which could effectively accelerate the hepatobiliary excretion of silica nanoparticles. Thus, the retention time of nanoparticles in the body could be adjusted by the manipulation of the surface charge.

3.2 Ultrasmall silica nanoparticles

Dye encapsulated ultra-small silica nanoparticles, termed Cornell dots (C dots), began clinical trials in 2011.[52] Bradbury and coworkers carried out a plethora of original studies on

the PET imaging of I^{124}-cRGDY-PEG-C dots (cRGDY = cyclic arginine-glycine-aspartic acid-tyrosine) in animal models and human body. This approach may be employed for cancer staging, lesion detection, and treatment administration in human. Furthermore, this PET-optical imaging agent has been approved by the US FDA Investigational New Drug (IND) for targeted molecular imaging.

In 2009, Burns *et al.* designed a new generation of fluorescent core/shell silica-based nanoparticles consisting of an organic dye Cy5 core and a silica shell.[53] To evaluate the effect of the probe size on the biodistribution and clearance, Cy5-containing core/shell silica nanoparticles with different HD (3.3 and 6.0 nm) were optimized by the hybrid silica technologies. As compared with small sized nanoparticles, the large nanoparticles exhibited longer half-life with more retention in initial organ (liver), thereby resulting in slower excretion from the body. To promote the development toward clinical applications, they then fabricated the next generation of dye-encapsulating silica nanoparticles, surface-functionalized with targeting peptides and radioiodine, named I^{124}-CRGDY-PEG-C dots **(Figure 8a,b)**.[54] This renally excretive agent efficiently achieved specific tumor-selective targeting and nodal mapping on melanoma models using mice and miniswine, which has been approved for the first-in-human clinical trial.

Due to its high biocompatibility and biodegradability, hyaluronic acid (HA) has been intensively studied as a drug delivery carrier with specific targeting to the liver.[55] Kim and coworkers reported a new type of HA-integrated ultrasmall silica nanoparticles (HA-SiNP) for specific delivery and imaging toward the diagnosis of liver disease.[56] HA having negative charges and SiNP showing strong PA signal in the NIR window could help the system avoid nonspecific binding and aid in visualizing the targeted delivery to liver tissue and the clearance from the body **(Figure 8c,d)**. After the injection of SiNP and HA-SiNP, the absorption spectra of the collected urine showed comparable results for these two types of nanoparticles, indicating that these nanoparticles could be cleared by urine from the body after the accumulation in the

liver on account of their ultrasmall sizes **(Figure 8e)**. The inductively coupled plasma-mass spectroscopy (ICP-MS) analysis showed no significant content of SiNP and HA-SiNP in the heart, kidney, lung, and liver **(Figure 8f)**. Therefore, the urine study and biodistribution analysis in major organs supported that HA-SiNP was biodegradable.

3.3 Regulating the degradability of silica by doping inorganic species

The tunability of the silica degradability by the means of inorganic doping has garnered widespread attention. Specific parameter adjustment for the decomposition of silica into silicic acid as well as the stability of metal ion or oxide doping from hydrolysis would affect the decomposition rate of silica nanoparticles. As such, it is of great concern as to how these parameters could influence the degradability of the materials in various media. Thus, the effect of inorganic doping (such as calcium, manganese and iron cations/oxides) into silica is discussed in this section.

Recently, several types of calcium-doped silica nanoparticles were designed for the regulation on the hydrolytic stability of the particle framework under acidic conditions. Zhang and coworkers reported degradable and acidic-responsive MSNs/hydroxyapatite (MSNs/HAP) hybrid nanoparticles by means of homogeneously merging calcium salt into silica nanoparticles.[57] The MSNs/HAP nanoparticles were able to dissociate into smaller fragments due to the removal of Ca^{2+} cations from the framework under acidic environments. Furthermore, *in vivo* distribution and degradation properties of these nanoparticles were also investigated. It was found that the nanoparticles injected were mainly distributed in the liver and spleen, consistent with previously reported biodistribution of silica nanoparticles. As compared to free MSNs, however, the silicon signal from the MSNs/HAP in the kidney showed an increased accumulation. This result may be due to that small fragments were accumulated in the kidney after the decomposition of MSNs/HAP, inducing the excretion *via* the renal clearance. In another work, a pH-responsive and biodegradable silica-calcium phosphate (CaP) nanocomposite was developed by Xu and coworkers, where CaP precursors (Ca^{2+} and $PO4^{3-}$)

were doped into the MSN framework by the one-step method during the growth process **(Figure 9a)**.[58] Due to rapid decomposition of CaP and a large amount of Ca^{2+} release from the framework structure of Si-O-Ca, the entire degradation process could almost be completed within 24 h under acidic pH **(Figure 9b,c)**.

Iron oxide was introduced into MSNs in order to enhance the biodegradability of the nanocarriers. Chou and coworkers designed a T1 contrast agent, *i.e.*, α-FeOOH nanocolloids with an ultrasmall size, which could be uniformly dispersed into the mesopores of worm-like mesoporous silica (WMSN) **(Figure 9d)**.[59] The human serum and FBS could promote the degradation of silica framework because of the presence of iron-chelating agents. Furthermore, the degradation of FeOOH/WMSN-PEG was much faster than that of WMSN-PEG when incubated with iron removing agents, indicating its potential biodegradability **(Figure 9e)**. This result was attributed to the chelating effect of biological ligands present in mammalian serum medium (*e.g.*, transferrin), which owned a formation constant of ~10^{20} with iron(III). The same research team later used a similar strategy to design a degradable FeOOH functionalized hollow MSNs for *in vivo* T1 magnetic resonance imaging (MRI).[60] The FeOOH functionalized hollow MSNs showed faster degradation in FBS than in phosphate buffered saline (PBS), which was again attributed to the presence of transferrin proteins in FBS. In addition, the incorporation of cations into silica nanoparticles could greatly enhance the degradation rate of nanoparticles. Trogeler *et. al.* doped iron(III) into hollow silica shells fabricated by the sol-gel approach.[61] Iron doped hollow nanoparticles were incubated with the iron chelators and mammalian serum to evaluate their degradability. Different chelating ligands (such as ethylenediaminetetraacetic acid), human serum, and FBS were all found to cause the collapse of the structure for the formation of ultrasmall silica clusters by the removal of iron(III).

Mn element has an irreplaceable role in the metabolism of the human body and can be efficiently excreted from the biological system, exhibiting low toxicity and high biosafety. It was confirmed that the -Mn-O- bond could be cleaved under the reducing or acidic

environments. Based on this information, Shi and coworkers developed manganese-doped hollow mesoporous silica nanoparticles (Mn-HMSNs) to greatly accelerate the fracture of the Si-O-Si bond within the MSN framework under either mild acidic or reducing conditions **(Figure 9f)**.[62] Abundant flaws within the framework were found after the destruction of the -Mn-O- bond to release Mn and Si ions **(Figure 9g,h)**, further inducing the framework degradation of Mn-HMSNs **(Figure 9i,j)**. On account of the release of free Mn ion, the T1-weighted MRI signal could be significantly enhanced for tumor-specific imaging. A high Si content in the urine was notable due to the fast degradation of PEG/Mn-HMSNs, generating small fragmented products that could be readily excreted through the renal metabolic pathway.

3.4 Regulating the degradability of silica by incorporating of organic moieties

The degradation and clearance of silica nanoparticles that were incorporated with organic moieties have also been studied. Some strategies include: (1) physical doping of organic molecules into the framework of silica nanoparticles to accelerate the hydrolytic degradation, (2) covalent doping of cleavable organically bridged silsesquioxanes into silica nanoparticles to enhance the degradation under the redox or enzymatic conditions, and (3) the self-assembly between triblock copolymers and silica precursors that can be rapidly cleared through the hepatobiliary excretion.

Zhang *et al.* prepared the SiO_2-drug composite nanoparticles by incorporating the drug molecules into the silica during the nanoparticle growth process **(Figure 10a)**.[63] Controllable release of drug could trigger the degradation of the SiO_2 nanocarrier. The degradation began from the center of the nanoparticles, ultimately leading to entire fragmentation. This design rendered simultaneous decomposition of the nanocarrier and the release of loaded drugs. The biodistribution study revealed that the injected SiO_2-drug nanoparticles accumulated primarily in the RES organs (liver and spleen). As compared to dense SiO_2-drug nanoparticles at 48 h after the injection, the drug diffusion induced decomposition of SiO_2-drug nanoparticles resulted in remarkedly reduced enrichment in the corresponding organs **(Figure 10b,c)**. The

same research team later introduced doubly loaded self-decomposable SiO_2 nanoparticles, in which two different loading mechanisms were used.[64] The drug molecules were first loaded during the growth of SiO_2 nanoparticles, and then the preloaded nanoparticles were dispersed into the drug solution for another round of drug loading. After the loaded drug was fully released, the self-decomposable SiO_2 nanocarrier would be decomposed into small fragments for easy excretion from the body through the renal system.

Relatively high concentration of some bio-reductants inside cancer cells has aroused intensive development of redox-responsive delivery systems. Glutathione (GSH) has greater concentration in tumor cells than in normal cells, which is ideal for GSH-triggered therapeutics in the treatment of cancer.[65] Covalent incorporation of redox-responsive bonds into the silica nanoparticles allows such bonds to be cleaved by GSH. Thus, the redox-triggered degradation of the silica framework could be applied for drug and gene delivery in cancer therapy. In 2014, Shi and coworkers reported organic-inorganic hybrid hollow mesoporous organosilica nanoparticles (HMONs) with alterable organic groups doped into the framework **(Figure 10d)**.[66] Such organic-inorganic hybridization offered a versatile method to realize different HMONs for various applications. In this study, HMONs integrated with phenylene and thioether groups in the framework were fabricated for loading the anticancer drug. The disulfide bonds within the structure of HMONs were highly responsive to the reducing condition for rapid release of loaded drug **(Figure 10e)**. Furthermore, HMONs also showed gradual biodegradation behavior under 10 mM GSH. Many therapeutic agents were loaded into such organosilica systems for different therapeutic applications, such as chemotherapy, radiotherapy, gene therapy, and sonodynamic therapy.[67] This strategy enabled concurrent stimuli-responsive drug delivery and degradability of the nanocarriers on account of the presence of intrinsic reducing microenvironment of tumor tissues.

The prodrug strategy was exploited by Lin *et al.*, in which a cisplatin-integrated polysilsesquioxane (PSQ) platform was designed for oxaliplatin delivery.[68] The PSQ

nanoparticles were stable at pH 7.4, while the Pt prodrug within the nanoparticle framework could be quickly reduced by the endogenous biomolecules (*e.g.*, GSH and cysteine) to release the toxic oxaliplatin. The PSQ nanoparticles were applied in xenograft tumor models *in vivo*, exhibiting significant efficacy to inhibit the tumor growth in comparison to free oxaliplatin. An enzyme responsive mechanism was also introduced into silica nanoparticles, where organic bonds were cleaved by the peculiar enzyme under the process of metabolism. Khashab and coworkers designed enzymatically degradable PSQ nanoparticles using the oxamide bridges present in the organosilica framework.[69] The degradability of nanoparticles was then tested in simulated biological solution. The results indicated that the nanoparticles were only degraded in the presence of trypsin enzyme in PBS. To overcome low mesoporosity, they developed oxamide phenylene-based mesoporous organosilica nanoparticles (MONs), prepared from the co-condensation of 1,4-bis(triethoxysilyl)-benzene and (N,N'-bis(3-(triethoxysilyl)-propyl)oxamide).[70] The capability of MONs to be degraded by trypsin was demonstrated using several techniques. These nanoparticles could not only undergo specific degradation when treated with trypsin, but also possess higher drug loading capacity of up to 84 wt%.

Some polymers were also reported to be used in the preparation of organic-inorganic hybrids with silica through different pathways, including layer-by-layer and surface-originated polymerization. For example, we prepared ultra-small silica-polymer hybrid nanodots (named as Sdots) through the self-assembly between a silica precursor and a triblock copolymer polyethylene oxide-poly(propylene oxide)-polyethylene oxide (PEO-PPO-PEO, **Figure 10f,g)**.[71] Upon i.v. injection, Sdots were mainly cleared from the body through hepatobiliary excretion within a short period **(Figure 10h-j)**. As compared to mushroom-like PEG modification, the brush-like PEG modification on Sdots provided significant stealth property, helping Sdots avoid the uptake by the RES as much as possible and ensure their rapid excretion. The brush-like PEG modified Sdots also had a prolonged blood circulation half-time and could effectively accumulate at tumor region through the EPR effect. However, the main disadvantage

of these Sdots was the lack of porous structures, thus limiting their drug loading capacity. In order to solve this issue, we further developed a polymer-silica nanohybrid (named as HPSN) with a hollow structure using a pore-expanding agent (volatile cyclohexane). The pore-expanding agent could be removed under mild conditions.[72] Chemotherapeutic drugs and photothermal agents were simultaneously loaded into the mesoporous structure of silica layer for combination therapy. The *in vivo* studies showed that HPSN could be rapidly excreted from the mouse body through the hepatobiliary pathway, therefore reducing the side effect of the loaded anticancer drugs.

In addition to silica nanoparticles, silicon nanoparticles could also be designed as excellent drug delivery vehicles for biomedical applications.[73] Lee and coworkers reported degradable hollow mesoporous silicon/carbon nanoparticles for pH-responsive, imaging-guided chemo-thermal combination therapy **(Figure 11a,b)**.[74] Having effective photothermal conversion efficiency and high drug loading capacity, the hollow mesoporous silicon/carbon nanoparticles could significantly kill cancer cells and eliminate tumors through chemo-thermal therapy. In order to study the biodegradability of the as-synthesized silicon/carbon nanoparticles, they examined the release of silicon from the nanoparticles into the PBS solution **(Figure 11c)**. It was found that only 0.35 wt% of silicon was released into PBS solution without shaking in one month. Conversely, 8.4 wt% of silicon was dissolved into PBS after one month shaking. Observations by scanning electron microscopy (SEM) and TEM revealed significant changes in the morphology of the silicon/carbon nanoparticles after shaking in PBS. These results indicate that the synthesized silicon/carbon nanoparticles were biodegradable carriers for drug delivery and cancer treatment.

4 Metallic and metal-containing nanoparticles

Metal, metal oxide, and other metal-related nanoparticles have been synthesized and used

for therapeutic and diagnostic purposes, which call for evaluation regarding the biodegradation and clearance pathways.[75] In previous sections, we already systematically discussed the biodistribution, pharmacokinetics, and clearance of metal-containing QDs. On account of potential applications in drug and protein delivery for cancer diagnosis and treatment, some traditional metal-containing nanomaterials including gold nanoparticles and metal oxides (such as γ-Fe_2O_3 and Fe_3O_4) have been studied for their toxicity and excretion pathways by many researchers.[76] For example, Cheheltani *et al.* synthesized sub-5.5 nm gold nanoparticles and incorporated them into a degradable polymer, poly-di(carboxylatophenoxy) phosphazene (PCPP), to prepare Au-PCPP nanocomposites **(Figure 12a)**.[77] The polymer could degrade into nontoxic byproducts and then release small-sized gold nanoparticles for the excretion **(Figure 12b-d)**. In this section, we introduce the detailed degradation and excretion behavior of some emerging metallic nanoparticles, including manganese dioxide (MnO_2), calcium carbonate ($CaCO_3$), tri-calcium phosphate ($Ca_3(PO_4)_2$), and transition metal dichalcogenides (TMDCs).

4.1 MnO_2 nanoparticles

A variety of different manganese oxide (MnO_2) nanostructures have been described to be biocompatible for biomedical applications because Mn element is a necessary trace element whose metabolism can be effectively controlled in the body.[78] It has been reported that MnO_2 nanostructures could be degraded by either acidic or redox (GSH) environments, releasing Mn^{2+} ions to increase the T1 magnetic resonance performance for specific tumor imaging.[79] Furthermore, MnO_2 nanostructures could relieve tumor hypoxia because it is capable of reacting with endogenous H_2O_2 to produce oxygen and water.[80] Such an effect significantly enhances the therapeutic outcome of oxygen-related treatments. MnO_2 nanoparticle could be completely decomposed into free Mn^{2+} ions that are quickly excreted by the kidney, leading to minimal long-term toxicity when they are utilized for *in vivo* studies.[78a]

Using a simple exfoliation method, Chen *et al.* reported an intelligent theranostic 2D MnO_2 nanosheets for pH-responsive T1 MRI and controllable drug delivery/release.[81] The loaded

drugs were released under a mildly acidic conditions with the dissociation of the drug-loaded MnO_2 nanosheets. The released Mn^{2+} ions from the gradually disintegrating MnO_2 nanosheets could be effectively excreted by the kidney, which solved the intricate degradation issue. Recently, Liu and coworkers prepared multifunctional platforms based on different MnO_2 nanostructures for tumor T1 MRI, tumor hypoxia relief, and improved cancer treatment efficacy. In their recent work, they developed a multifunctional pH/H_2O_2-responsive human serum albumin (HSA)-coated MnO_2 nanoparticles (HMCP) through HSA-based biomineralization of Mn^{2+} ions in alkaline conditions **(Figure 13a)**.[82] In this therapeutic system, a photosensitizer and a *cis*-platinum prodrug were pre-modified with HSA, which were then employed as the template to produce the MnO_2 nanoclusters. On one hand, such MnO_2-based nanoparticles could generate oxygen *in situ* after the reaction with endogenous H_2O_2 in tumor microenvironment, enhancing the performance of hypoxia-associated resistance of photodynamic therapy. On the other hand, these nanoparticles could gradually be decomposed into ultrasmall HSA-drug complexes (< 10 nm), which greatly increased the intratumoral penetration of released ultrasmall species **(Figure 13b-d)**. They also reported biodegradable hollow MnO_2 nanostructures for tumor-specific drug delivery and controllable release, tumor microenvironment-responsive production of oxygen to overcome the hypoxia of tumors, and enhanced combination therapy with imaging capability **(Figure 13e,f)**.[83] It was demonstrated that the combination therapy based on this hollow MnO_2 nanoshells significantly induced the anti-tumor immunity, which inhibited the distant tumor without light exposure through a remarkable abscopal effect with the incorporation of programmed death-ligand 1 (PD-L1) **(Figure 13g)**. The MRI demonstrated that strong T1 signals could be observed in the kidney of mice, suggesting fast renal excretion of released Mn^{2+} ions from the nanoplatform.

4.2 Calcium-based biomineralized nanomaterials

Calcium-based nanoparticles, such as calcium carbonate ($CaCO_3$) and tri-calcium phosphate ($Ca_3(PO_4)_2$), have shown to be promising candidates for biomedical applications

because of their high biocompatibility, biodegradability and responsiveness to pH.[84] As a familiar inorganic material in the nature, $CaCO_3$ is stable under neutral pH and dissociates into Ca^{2+} ions and CO_2 under acidic pH conditions, which can possibly be used in pH-responsive drug/gene delivery. Liu and coworkers reported monodispersed $CaCO_3$ nanoparticles as an intelligent nanocarrier for effective loading of different model drugs.[85] The obtained nanoparticles were easily decomposed under mild acidic condition, efficiently releasing the loaded drugs. Surprisingly, these nanoparticles exhibited a pH-dependent T1 magnetic resonance signal enhancement due to the release of Ce6 (Mn), which could be used for monitoring real-time drug release. They also developed $CaCO_3$-PDA-PEG hollow nanoparticles using a dopamine-modulated biomineralization method, showing fast decomposition under a mild acidic condition **(Figure 14a)**.[86] The fluorescence of loaded photosensitizer (Ce6), which was initially quenched by PDA under pH 7.4, exhibited the fluorescence recovery and thus significantly increased the singlet oxygen production under reduced pH **(Figure 14b,c)**. Furthermore, the fluorescence signals in the kidney were relatively high, while the remaining nanoparticles in the liver and kidney quickly reduced upon time, suggesting that nanoparticles might be cleared from the body by the renal clearance **(Figure 14d)**.

CaP nanoparticles are also nearly ideal carriers for anticancer drug or siRNA delivery because of their biodegradability and pH responsiveness. CaP is able to load various types of drug molecules in its rigid framework to completely prevent the early leakage of drugs at pH ~ 7.4 until releasing the calcium and phosphate ions in acidic environment. For example, Xu *et al.* developed biodegradable CaP-doped hollow mesoporous copper sulfide (CaNG) for tumor-specific synergistic therapy, releasing Ca^{2+} ions directly in the lysosomes.[87] The *in vitro* experiments indicated that a large amount of released Ca^{2+} ions directly flowed to mitochondria, resulting in the downregulation of Bcl-2 and adenosine tri-phosphate and the upregulation of Caspase-3 and cytochrome C to induce the cell apoptosis. TEM results showed that almost all

nanoparticles degraded into smaller fragments at pH 5.0, suggesting the complete Ca^{2+} release after the incubation for 1 h. CaNG would disintegrate into small sized nanoparticles in the process of metabolism, reducing its retention time *in vivo*. In 2012, Huang and coworkers reported lipid coated calcium phosphate (LCP) nanoparticles, showing efficient gene silencing in animal study. They have conducted detailed research on LCP, owing to its advantages in loading different types of therapeutic species, such as anticancer drugs, siRNA/DNA, and peptides.[88] It was assumed that LCP could disassemble in low pH environment of endosome after being endocytosed by cells, inducing the swelling of endosome and the release of the loaded drugs.

4.3 Transition metal dichalcogenides

As a type of emerging 2D nanomaterials, various TMDCs with extraordinary physicochemical properties have been developed to present promising applications in many fields including nanomedicine.[89] Therefore, the biodistribution, toxicology profiles and metabolic pathway of different TMDCs should be carefully studied in order to ensure that they have low toxicity and rapid excretion for theranostics.

Zhou *et al.* prepared multifunctional ultrasmall copper sulfide nanodots (CuS NDs) based on a chemical reaction of Cu^{2+} ion with S^{2-} ion under the incorporation of polyvinylpyrrolidone **(Figure 15a)**.[90] The CuS NDs showed an HD of less than 6 nm, and could be stably labelled with copper-64 radioisotope to realize PET imaging. Interestingly, ~ 95 % of CuS NDs were cleared intact from the urinary system within one day, simultaneously revealing minimal retention in the liver and spleen **(Figure 15b)**. Its photothermal conversion efficiency was also high, which could be used for photothermal therapy to efficiently inhibit the tumor growth *in vivo* **(Figure 15c)**.

The biodegradability and prolonged retention in organs for TMDCs with different structures were partially explored. Zhang and coworkers proposed $MoTe_2$ nanosheets as a multifunctional therapeutic agent of cancer.[91] These nanosheets were relatively stable under

normal physiological conditions, but would degrade under NIR laser irradiation and be readily removed from the body, decreasing their long-time toxicity. Song *et al.* synthesized molybdenum oxide (MoOx) nanosheets with high NIR absorbance and pH-responsive oxidative degradation properties. The nanosheets could retain their stability under acidic pH, but be degraded at physiological pH **(Figure 15d-f)**.[11] Therefore, PEG-modified MoOx (MoOx-PEG) was easily degraded in organs and excreted from the mouse, while exhibiting longer accumulation in tumors with acidic microenvironment for efficient photothermal therapy **(Figure 15g,h)**. Except for 2D TMDC nanosheets, ultrasmall TMDC dots have also been developed for applications of optical imaging and cancer therapy. In one recent study, cysteine-functionalized MoS_2 nanodots were prepared by a "top-down" method using ultrasonication and gradient centrifugation for applications as radioprotectors.[92] Approximately 80 % of cysteine-modified MoS_2 nanodots were cleared *via* the bladder within one day and exhibited no obvious toxicity even at a high injection dose. Liu and coworkers reported ultrasmall MoS_2 dots using a facile "bottom-up" approach, which revealed obvious photothermal ablation of cancer cells.[93] Compared with large sized conventional MoS_2 nanoflakes, the GSH-modified MoS_2 showed efficient renal clearance, where the injected nanodots were almost cleared within one week.

4.4 Other metal-containing nanoparticles

Clay nanopartcles, such as layered double hydroxide (LDH) and hectorite (HEC), are considered promising candidates for imaging, treatment, and vaccine applications, primarily because of their low toxicity, high biocompatibility, and other properties suitable for biomedicine.[94] LDH is hydrotalcite-like or anionic clay, represented by the chemical formula of $[M^{II}_{1-x}M^{III}_{x}(OH)_2]^{x+}(A^{n-})_{x/n}\cdot mH_2O$, where M^{II} is a divalent metal ion such as Mg^{2+}, Zn^{2+}, or Ca^{2+}, M^{III} is a trivalent metal ion like Al^{3+}, Fe^{3+} or Cr^{3+}, and A^{n-} is an anion.[95] Thus, LDH shows representative metal hydroxide-like properties and a clay-like layered crystalline structure. On the other hand, HEC is layered aluminosilicate cationic clay nanoparticles with

negative charge. This clay material has recently been studied as a carrier for the delivery of anticancer drugs with very low toxicity.[96] Due to their safety and reliability, researchers have used LDH and HEC as potential adjuvants in generating effective immune responses.[97]

Xu and coworkers demonstrated that LDH and HEC-antigen nanocomplexes could form loose agglomerates in the culture medium and loose structural nodules after subcutaneous injection in the tissue **(Figure 16a)**.[98] These clay nanoadjuvants could be used as a depot for up to 35 days before they got biodegraded. Clay nanoparticles continuously recruit immune cells to the depot for up to one month, stimulating stronger immune response than the two adjuvants approved by the FDA, *i.e.*, Alum and QuilA. Since the biodegradability of clay materials is of paramount importance for biological applications, the degradation of the formed nodules was studied **(Figure 16b-e)**. The amount of clay nanoparticles remaining in the nodules was quantified by inductively coupled plasma optical emission spectrometry (ICP-OES). The results showed that 36 % and 50 % of injected LDH and HEC nanoparticles were biodegraded after 35 days. At the same time, approximately 51 % and 71 % of the antigens were released from LDH and HEC nodules, respectively. These results indicate that the nodules formed by these nanoparticles were slowly degradable for sustained release of antigens.

5 Long-term retention of inorganic nanoparticles

To minimize nonspecific accumulation of inorganic nanoparticles in RES organs and reduce their potential toxicity, we herein summarized diverse types of biodegradable and clearable inorganic nanomaterials for biological applications. However, some inorganic nanomaterials are difficult to be rapidly degraded or metabolized in the body. Liu and coworkers systematically investigated three typical TMDCs in animal models **(Figure 17a)**, including tungsten dichalcogenide (WS_2), molybdenum dichalcogenide (MoS_2), and titanium dichalcogenide (TiS_2).[99] These three types of PEG modified TMDCs mainly accumulated in

RES organs (liver and spleen) after i.v. injection. While MoS_2-PEG underwent the degradation easily and was excreted within one month, significant amounts of W and Ti were retained in liver and spleen even after one month. Based on these observations, they concluded that the differences in the excretion behavior of these three types of TMDCs were due to their different chemical properties. WS_2 was very stable in physiological environment, decreasing its degradation **(Figure 17c,f)**. Therefore, WS_2-PEG would retain in the RES organs for a long time without the excretion after i.v. injection. TiS_2 was unstable and would gradually be oxidized into water-insoluble TiO_2 that was also difficult to be excreted from the mice (**Figure 17d,g**). MoS_2 could be oxidized and transformed into water-soluble Mo^{VI}-oxide species, which was then quickly excreted from the body through urine and feces **(Figure 17b,e)**.

Liu and coworkers reported two different surface-modified upconversion nanoparticles (UCNPs) by poly(acrylic acid) (PAA) and PEG for animal studies.[100] Similar to the test results of many inorganic nanoparticles, the UCNPs abundantly accumulated in the RES system, such as the liver and spleen, after i.v. injection. The quantitative analysis indicated that the UCNPs would remain in the RES system for a long period (3 months) with only partial excretion. On the other hand, Xiong *et al.* developed PAA-coated ultrasmall UCNPs (diameter = 10 nm), which could be completely excreted from the body of mice after 115 days.[101] The size of nanoparticles plays an important role for their *in vivo* behavior including the excretion. The size difference of UCNPs between the two studies may be the cause of their different excretion fate.

Several research groups have studied the biodistribution of carbon nanotubes (CNT) using different tracking modalities to quantitatively or qualitatively test its accumulation. Sun *et al.* systematically investigated the biodistribution of pristine single-walled carbon nanotubes (SWNTs) in mice through the tail vein injection.[102] SWNTs were quickly cleared from the bloodstream and distributed throughout most of the organs within a day, but preferentially accumulated in the liver, spleen and lung. It is important to note that SWNTs would remain in these organs for a long time (over 28 days) at a relatively high level of accumulation. It was

found that the surface chemistry of CNT was critical for their animal behavior. Dai and coworkers utilized Raman spectroscopy and Raman imaging to measure the blood circulation time of different PEG coated SWNTs and their biodistribution in major organs of mice over several months.[103] The results demonstrated that PEG functionalized SWNTs afforded longer blood circulation, lowed RES uptake, and relatively quick clearance from organs and excretion from the mice.

Based on these detailed discussions, there are some strategies to degrade or eliminate inorganic nanoparticles during the biomedical applications. (1) According to distinctive chemical properties, changes in the elemental composition of inorganic nanoparticles could be harnessed to achieve faster degradation or excretion from the body. (2) Smaller sized nanoparticles could be used, which are expected to show faster excretion rates as compared to larger ones. (3) Modifying the surface of inorganic nanoparticles with biocompatible polymers (such as PEG) to reduce the uptake of the RES organs and achieve faster clearance from the body would be another useful strategy.

6 Experimental tools

In order to study and understand the degradability and clearance of inorganic nanoparticles, different kinds of characterization techniques are required. These techniques are employed to investigate the stability of nanomaterials in different physiological environments, the biodistribution in various organs, and their metabolic pathways. We summarize the following characterization methods to explore the degradation and metabolism of inorganic nanoparticles *in vitro* and *in vivo*.

Dynamic light scattering (DLS): measuring the size change of inorganic nanoparticles in physiological environment. UV-Vis-NIR absorbance spectra: observing the degradation rate of some inorganic nanomaterials with absorption changes. SEM and TEM: observing changes in

morphology and size of nanomaterials *in vitro* and distribution in various organs. Powder X-ray diffraction (XRD) measurements: observing the change in pore/crystal structures. Brunauer-Emmett-Teller (BET) surface area analysis: detecting changes in BET surface area and pore volume. X-ray photoelectron spectroscopy (XPS): detecting changes in the valence state of elements contained in nanomaterials. ICP measurement: quantitatively studying the biodistribution of nanomaterials in different organs and their mass in metabolites (*i.e.*, feces and urinary). *In vivo* imaging (such as fluorescence imaging, MRI, and PET imaging): qualitative analysis on the biodistribution of nanoparticles in various organs.

7 Conclusions and future perspectives

In conclusion, we have summarized various factors that greatly influence the degradability and clearance of different inorganic nanoparticles, including quantum dots, silica nanoparticles, and metallic and metal-containing nanoparticles. These studies aim to address long-term challenges for future clinical translation of inorganic nanoparticles. The size, morphology, surface modification, composition, and surface area are significant factors, which need to be considered in the design of biodegradable and clearable inorganic nanoparticles. These various types of inorganic nanoparticles could be used for different modes of imaging and multiple effective treatments while getting rapidly decomposed or metabolized to reduce their toxicity, placing high expectation for the diagnosis and treatment of serious diseases.

Although preliminary results have shown that these inorganic nanoparticles with degradability and clearance properties are highly promising for future disease treatment, there are still many crucial issues that have to be addressed before clinical applications can be achieved. Many inorganic nanoparticles are metabolized through the kidney after their degradation into small sized fragments. On the other hand, the generated ions, especially heavy metals, may cause the damage or toxicity to the related organs during the excretion. Therefore,

it is necessary to systematically study the toxicity of these nanomaterials to organs during the metabolism. While rapid clearance significantly reduces the toxic effect of nanomaterials on the body, how to achieve their efficient accumulation in the tumor or related lesions is a great challenge. In the future studies, more effective strategies need to be designed to enhance the accumulation of inorganic nanoparticles in the process of metabolism. Future degradable and clearable inorganic nanoparticles should not only be limited to these reported materials, expanding the inventory of such nanoparticles with diverse biomedical functionalities will be a research focus. Once the inorganic nanoparticles with different components are designed, we will be able to gain deeper understanding about the differences in metabolic processes between these inorganic materials. Among the reported inorganic materials, the C dots have been approved by the US FDA as a new generation of therapeutic agent for in-human clinical trials. Thus, we believe that these degradable or clearable inorganic materials have a bright future for practical biomedical uses.

Acknowledgements

This research is supported by the Singapore Academic Research Fund (No. RG11/17 and RG114/17), the Singapore Agency for Science, Technology and Research (A*STAR) AME IRG grant (No. A1883c0005), and the Singapore National Research Foundation Investigatorship (No. NRF-NRFI2018-03).

References

[1] a) G. Yang, H. Gong, T. Liu, X. Sun, L. Cheng, Z. Liu, *Biomaterials* **2015**, *60*, 62; b) G. Yang, H. Gong, X. Qian, P. Tan, Z. Li, T. Liu, J. Liu, Y. Li, Z. Liu, *Nano Res.* **2015**, *8*, 751; c) W. R. Sanhai, J. H. Sakamoto, R. Canady, M. Ferrari, *Nat. Nanotechnol.* **2008**, *3*, 242; d) D. Ho, C.-H. K. Wang, E. K.-H. Chow, *Sci. Adv.* **2015**, *1*, e1500439; e) G. Tian, Z. Gu, L. Zhou, W. Yin, X. Liu, L. Yan, S. Jin, W. Ren, G. Xing, S. Li, Y. Zhao, *Adv. Mater.* **2012**, *24*, 1226.

[2] a) K. T. Nguyen, Y. Zhao, *Acc. Chem. Res.* **2015**, *48*, 3016; b) X. Ma, Y. Zhao, *Chem. Rev.* **2015**, *115*, 7794; c) T. Sun, Y. S. Zhang, B. Pang, D. C. Hyun, M. Yang, Y. Xia, *Angew. Chem. Int. Ed.* **2014**, *53*, 12320; d) E. B. Ehlerding, F. Chen, W. Cai, *Adv. Sci.* **2016**, *3*, 1500223; e) X.-D. Xu, X. Li, H. Chen, Q. Qu, L. Zhao, H. Ågren, Y. Zhao, *Small* **2015**, *11*, 5901.

[3] a) G. Yang, X. Sun, J. Liu, L. Feng, Z. Liu, *Adv. Funct. Mater.* **2016**, *26*, 4722; b) Q. Zhang, F. Liu, K. T. Nguyen, X. Ma, X. Wang, B. Xing, Y. Zhao, *Adv. Funct. Mater.* **2012**, *22*, 5144; c) H. Yan, C. Teh, S. Sreejith, L. Zhu, A. Kwok, W. Fang, X. Ma, K. T. Nguyen, V. Korzh, Y. Zhao, *Angew. Chem. Int. Ed.* **2012**, *51*, 8373.

[4] a) S. Y. Lim, W. Shen, Z. Gao, *Chem. Soc. Rev.* **2015**, *44*, 362; b) X. Dai, Z. Zhang, Y. Jin, Y. Niu, H. Cao, X. Liang, L. Chen, J. Wang, X. Peng, *Nature* **2014**, *515*, 96; c) Z. Sun, H. Xie, S. Tang, X.-F. Yu, Z. Guo, J. Shao, H. Zhang, H. Huang, H. Wang, P. K. Chu, *Angew. Chem. Int. Ed.* **2015**, *127*, 11688.

[5] a) Z. Liu, J. T. Robinson, S. M. Tabakman, K. Yang, H. Dai, *Mater. Today* **2011**, *14*, 316; b) K. Yang, S. Zhang, G. Zhang, X. Sun, S.-T. Lee, Z. Liu, *Nano Lett.* **2010**, *10*, 3318; c) G. Gonçalves, M. Vila, M.-T. Portolés, M. Vallet-Regi, J. Gracio, P. A. A. P. Marques, *Adv. Healthcare Mater.* **2013**, *2*, 1072.

[6] a) G. Yang, L. Xu, J. Xu, R. Zhang, G. Song, Y. Chao, L. Feng, F. Han, Z. Dong, B. Li, Z. Liu, *Nano Lett.* **2018**, *18*, 2475; b) G. Yang, R. Zhang, C. Liang, H. Zhao, X. Yi, S. Shen, K. Yang, L. Cheng, Z. Liu, *Small* **2018**, *14*, 1702664; c) T. Y. Ohulchanskyy, I. Roy, L. N. Goswami, Y. Chen, E. J. Bergey, R. K. Pandey, A. R. Oseroff, P. N. Prasad, *Nano Lett.* **2007**, *7*, 2835.

[7] a) W. Lin, Y.-w. Huang, X.-D. Zhou, Y. Ma, *Toxicol. Appl. Pharm.* **2006**, *217*, 252; b) S. J. Soenen, P. Rivera-Gil, J.-M. Montenegro, W. J. Parak, S. C. De Smedt, K. Braeckmans, *Nano Today* **2011**, *6*, 446; c) B. Fadeel, A. E. Garcia-Bennett, *Adv. Drug Delivery Rev.* **2010**, *62*, 362; d) A. Elsaesser, C. V. Howard, *Adv. Drug Delivery Rev.* **2012**, *64*, 129.

[8] H. Soo Choi, W. Liu, P. Misra, E. Tanaka, J. P. Zimmer, B. Itty Ipe, M. G. Bawendi, J. V. Frangioni, *Nat. Biotechnol.* **2007**, *25*, 1165.

[9] a) M. Yu, J. Zheng, *ACS Nano* **2015**, *9*, 6655; b) J.-H. Park, L. Gu, G. von Maltzahn, E. Ruoslahti, S. N. Bhatia, M. J. Sailor, *Nat. Mater.* **2009**, *8*, 331; c) C. R. Kaiser, M. L. Flenniken, E. Gillitzer, A. L. Harmsen, A. G. Harmsen, M. A. Jutila, T. Douglas, M. J. Young, *Int. J. Nanosci.* **2007**, *2*, 715.

[10] a) C. Zhou, M. Long, Y. Qin, X. Sun, J. Zheng, *Angew. Chem. Int. Ed.* **2011**, *123*, 3226; b) J. Liu, M. Yu, C. Zhou, S. Yang, X. Ning, J. Zheng, *J. Am. Chem. Soc.* **2013**, *135*, 4978.

[11] G. Song, J. Hao, C. Liang, T. Liu, M. Gao, L. Cheng, J. Hu, Z. Liu, *Angew. Chem. Int. Ed.* **2016**, *55*, 2122.

[12] a) J. Liu, M. Yu, C. Zhou, J. Zheng, *Mater. Today* **2013**, *16*, 477; b) H. Omar, J. G. Croissant, K. Alamoudi, S. Alsaiari, I. Alradwan, M. A. Majrashi, D. H. Anjum, P. Martins, R. Laamarti, J. Eppinger, B. Moosa, A. Almalik, N. M. Khashab, *J. Controlled Release* **2017**, *259*, 187; c) S. Yang, S. Sun, C. Zhou, G. Hao, J. Liu, S. Ramezani, M.

Yu, X. Sun, J. Zheng, *Bioconjugate Chem.* **2015**, *26*, 511; d) J. G. Croissant, Y. Fatieiev, N. M. Khashab, *Adv. Mater.* **2017**, *29*, 1604634.

[13] a) P. Juzenas, W. Chen, Y.-P. Sun, M. A. N. Coelho, R. Generalov, N. Generalova, I. L. Christensen, *Adv. Drug Delivery Rev.* **2008**, *60*, 1600; b) V. Bagalkot, L. Zhang, E. Levy-Nissenbaum, S. Jon, P. W. Kantoff, R. Langer, O. C. Farokhzad, *Nano Lett.* **2007**, *7*, 3065; c) J. Ge, M. Lan, B. Zhou, W. Liu, L. Guo, H. Wang, Q. Jia, G. Niu, X. Huang, H. Zhou, X. Meng, P. Wang, C.-S. Lee, W. Zhang, X. Han, *Nat. Commun.* **2014**, *5*, 4596.

[14] a) Y. Zheng, S. Gao, J. Y. Ying, *Adv. Mater.* **2007**, *19*, 376; b) Y.-S. Liu, Y. Sun, P. T. Vernier, C.-H. Liang, S. Y. C. Chong, M. A. Gundersen, *J. Phys. Chem. C* **2007**, *111*, 2872; c) Y. He, H.-T. Lu, L.-M. Sai, Y.-Y. Su, M. Hu, C.-H. Fan, W. Huang, L.-H. Wang, *Adv. Mater.* **2008**, *20*, 3416.

[15] a) T. T. Tan, S. T. Selvan, L. Zhao, S. Gao, J. Y. Ying, *Chem. Mater.* **2007**, *19*, 3112; b) M. Ibáñez, R. Zamani, S. Gorsse, J. Fan, S. Ortega, D. Cadavid, J. R. Morante, J. Arbiol, A. Cabot, *ACS Nano* **2013**, *7*, 2573; c) L. Sun, L. Bao, B.-R. Hyun, A. C. Bartnik, Y.-W. Zhong, J. C. Reed, D.-W. Pang, H. D. Abruña, G. G. Malliaras, F. W. Wise, *Nano Lett.* **2009**, *9*, 789.

[16] a) Z. Kang, Y. Liu, C. H. A. Tsang, D. D. D. Ma, X. Fan, N.-B. Wong, S.-T. Lee, *Adv. Mater.* **2009**, *21*, 661; b) K. Hola, Y. Zhang, Y. Wang, E. P. Giannelis, R. Zboril, A. L. Rogach, *Nano Today* **2014**, *9*, 590; c) F. Erogbogbo, C.-A. Tien, C.-W. Chang, K.-T. Yong, W.-C. Law, H. Ding, I. Roy, M. T. Swihart, P. N. Prasad, *Bioconjugate Chem.* **2011**, *22*, 1081.

[17] a) W. Dai, H. Dong, B. Fugetsu, Y. Cao, H. Lu, X. Ma, X. Zhang, *Small* **2015**, *11*, 4158; b) H. Dong, S. Tang, Y. Hao, H. Yu, W. Dai, G. Zhao, Y. Cao, H. Lu, X. Zhang, H. Ju, *ACS Appl. Mater. Interfaces* **2016**, *8*, 3107; c) Y. Yong, X. Cheng, T. Bao, M. Zu, L. Yan, W. Yin, C. Ge, D. Wang, Z. Gu, Y. Zhao, *ACS Nano* **2015**, *9*, 12451.

[18] a) S. Zhu, Q. Meng, L. Wang, J. Zhang, Y. Song, H. Jin, K. Zhang, H. Sun, H. Wang, B. Yang, *Angew. Chem. Int. Ed.* **2013**, *125*, 4045; b) L. Cao, X. Wang, M. J. Meziani, F. Lu, H. Wang, P. G. Luo, Y. Lin, B. A. Harruff, L. M. Veca, D. Murray, S.-Y. Xie, Y.-P. Sun, *J. Am. Chem. Soc.* **2007**, *129*, 11318; c) T. Feng, X. Ai, H. Ong, Y. Zhao, *ACS Appl. Mater. Interfaces* **2016**, *8*, 18732.

[19] a) T. Feng, X. Ai, G. An, P. Yang, Y. Zhao, *ACS Nano* **2016**, *10*, 4410; b) P. Huang, J. Lin, X. Wang, Z. Wang, C. Zhang, M. He, K. Wang, F. Chen, Z. Li, G. Shen, D. Cui, X. Chen, *Adv. Mater.* **2012**, *24*, 5104.

[20] S.-T. Yang, L. Cao, P. G. Luo, F. Lu, X. Wang, H. Wang, M. J. Meziani, Y. Liu, G. Qi, Y.-P. Sun, *J. Am. Chem. Soc.* **2009**, *131*, 11308.

[21] X. Huang, F. Zhang, L. Zhu, K. Y. Choi, N. Guo, J. Guo, K. Tackett, P. Anilkumar, G. Liu, Q. Quan, H. S. Choi, G. Niu, Y.-P. Sun, S. Lee, X. Chen, *ACS Nano* **2013**, *7*, 5684.

[22] N. Licciardello, S. Hunoldt, R. Bergmann, G. Singh, C. Mamat, A. Faramus, J. L. Z. Ddungu, S. Silvestrini, M. Maggini, L. De Cola, H. Stephan, *Nanoscale* **2018**, *10*, 9880.

[23] S. Wang, C. Li, M. Qian, H. Jiang, W. Shi, J. Chen, U. Lächelt, E. Wagner, W. Lu, Y. Wang, R. Huang, *Biomaterials* **2017**, *141*, 29.

[24] C. Lee, W. Kwon, S. Beack, D. Lee, Y. Park, H. Kim, S. K. Hahn, S.-W. Rhee, C. Kim, *Theranostics* **2016**, *6*, 2196.

[25] D. Iannazzo, I. Ziccarelli, A. Pistone, *J. Mater. Chem. B* **2017**, *5*, 6471.

[26] M. Nurunnabi, Z. Khatun, K. M. Huh, S. Y. Park, D. Y. Lee, K. J. Cho, Y.-k. Lee, *ACS Nano* **2013**, *7*, 6858.

[27] M. Nurunnabi, Z. Khatun, M. Nafiujjaman, D.-g. Lee, Y.-k. Lee, *ACS Appl. Mater. Interfaces* **2013**, *5*, 8246.

[28] Y. Chong, Y. Ma, H. Shen, X. Tu, X. Zhou, J. Xu, J. Dai, S. Fan, Z. Zhang, *Biomaterials* **2014**, *35*, 5041.

[29] a) F. Erogbogbo, K.-T. Yong, I. Roy, G. Xu, P. N. Prasad, M. T. Swihart, *ACS Nano*

2008, *2*, 873; b) J. Li, J.-J. Zhu, *Analyst* **2013**, *138*, 2506.
[30] C. Tu, X. Ma, A. House, S. M. Kauzlarich, A. Y. Louie, *ACS Med. Chem. Lett.* **2011**, *2*, 285.
[31] J. L. May, F. Erogbogbo, K.-T. Yong, H. Ding, W.-C. Law, M. T. Swihart, P. N. Prasad, *J. Solid Tumors* **2012**, *2*, 24.
[32] a) W. Zhang, G. Chen, J. Wang, B.-C. Ye, X. Zhong, *Inorg. Chem.* **2009**, *48*, 9723; b) W. W. Yu, E. Chang, R. Drezek, V. L. Colvin, *Biochem. Biophys. Res. Commun.* **2006**, *348*, 781.
[33] W. Liu, H. S. Choi, J. P. Zimmer, E. Tanaka, J. V. Frangioni, M. Bawendi, *J. Am. Chem. Soc.* **2007**, *129*, 14530.
[34] N. Ma, A. F. Marshall, S. S. Gambhir, J. Rao, *Small* **2010**, *6*, 1520.
[35] a) X. Ma, Q. Qu, Y. Zhao, *ACS Appl. Mater. Interfaces* **2015**, *7*, 10671; b) Y. Zhao, Z. Luo, M. Li, Q. Qu, X. Ma, S.-H. Yu, Y. Zhao, *Angew. Chem. Int. Ed.* **2015**, *54*, 919; c) Z. Luo, Y. Hu, K. Cai, X. Ding, Q. Zhang, M. Li, X. Ma, B. Zhang, Y. Zeng, P. Li, J. Li, J. Liu, Y. Zhao, *Biomaterials* **2014**, *35*, 7951.
[36] a) F. Tang, L. Li, D. Chen, *Adv. Mater.* **2012**, *24*, 1504; b) Z. Li, J. C. Barnes, A. Bosoy, J. F. Stoddart, J. I. Zink, *Chem. Soc. Rev.* **2012**, *41*, 2590; c) G. Yang, J. Liu, Y. Wu, L. Feng, Z. Liu, *Coord. Chem. Rev.* **2016**, *320-321*, 100; d) Z. Luo, X. Ding, Y. Hu, S. Wu, Y. Xiang, Y. Zeng, B. Zhang, H. Yan, H. Zhang, L. Zhu, J. Liu, J. Li, K. Cai, Y. Zhao, *ACS Nano* **2013**, *7*, 10271.
[37] a) P. J. Kempen, S. Greasley, K. A. Parker, J. L. Campbell, H.-Y. Chang, J. R. Jones, R. Sinclair, S. S. Gambhir, J. V. Jokerst, *Theranostics* **2015**, *5*, 631; b) Q. Zhang, C. Shen, N. Zhao, F.-J. Xu, *Adv. Funct. Mater.* **2017**, *27*, 1606229.
[38] a) F. Lu, S.-H. Wu, Y. Hung, C.-Y. Mou, *Small* **2009**, *5*, 1408; b) D. Napierska, L. C. J. Thomassen, V. Rabolli, D. Lison, L. Gonzalez, M. Kirsch-Volders, J. A. Martens, P. H. Hoet, *Small* **2009**, *5*, 846; c) Q. Zhang, X. Wang, P.-Z. Li, K. T. Nguyen, X.-J. Wang, Z. Luo, H. Zhang, N. S. Tan, Y. Zhao, *Adv. Funct. Mater.* **2014**, *24*, 2450.
[39] H. Yamada, C. Urata, Y. Aoyama, S. Osada, Y. Yamauchi, K. Kuroda, *Chem. Mater.* **2012**, *24*, 1462.
[40] G. Chen, Z. Teng, X. Su, Y. Liu, G. Lu, *J. Biomed. Nanotechnol.* **2015**, *11*, 722.
[41] Q. He, Z. Zhang, F. Gao, Y. Li, J. Shi, *Small* **2011**, *7*, 271.
[42] a) R. Toy, P. M. Peiris, K. B. Ghaghada, E. Karathanasis, *Nanomedicine* **2014**, *9*, 121; b) N. P. Truong, M. R. Whittaker, C. W. Mak, T. P. Davis, *Expert Opin. Drug Deliv.* **2015**, *12*, 129.
[43] X. Huang, L. Li, T. Liu, N. Hao, H. Liu, D. Chen, F. Tang, *ACS Nano* **2011**, *5*, 5390.
[44] N. Hao, H. Liu, L. Li, D. Chen, L. Li, F. Tang, *J. Nanosci. Nanotechnol.* **2012**, *12*, 6346.
[45] V. Cauda, C. Argyo, T. Bein, *J. Mater. Chem.* **2010**, *20*, 8693.
[46] X. He, H. Nie, K. Wang, W. Tan, X. Wu, P. Zhang, *Anal. Chem.* **2008**, *80*, 9597.
[47] Y. Choi, J. E. Lee, J. H. Lee, J. H. Jeong, J. Kim, *Langmuir* **2015**, *31*, 6457.
[48] I. Izquierdo-Barba, M. Colilla, M. Manzano, M. Vallet-Regí, *Microporous Mesoporous Mat.* **2010**, *132*, 442.
[49] D. Shen, J. Yang, X. Li, L. Zhou, R. Zhang, W. Li, L. Chen, R. Wang, F. Zhang, D. Zhao, *Nano Lett.* **2014**, *14*, 923.
[50] Q. He, J. Shi, M. Zhu, Y. Chen, F. Chen, *Microporous Mesoporous Mat.* **2010**, *131*, 314.
[51] J. S. Souris, C.-H. Lee, S.-H. Cheng, C.-T. Chen, C.-S. Yang, J.-a. A. Ho, C.-Y. Mou, L.-W. Lo, *Biomaterials* **2010**, *31*, 5564.
[52] E. Phillips, O. Penate-Medina, P. B. Zanzonico, R. D. Carvajal, P. Mohan, Y. Ye, J. Humm, M. Gönen, H. Kalaigian, H. Schöder, H. W. Strauss, S. M. Larson, U. Wiesner, M. S. Bradbury, *Sci. Transl. Med.* **2014**, *6*, 260ra149.
[53] A. A. Burns, J. Vider, H. Ow, E. Herz, O. Penate-Medina, M. Baumgart, S. M. Larson, U. Wiesner, M. Bradbury, *Nano Lett.* **2009**, *9*, 442.

[54] M. Benezra, O. Penate-Medina, P. B. Zanzonico, D. Schaer, H. Ow, A. Burns, E. DeStanchina, V. Longo, E. Herz, S. Iyer, J. Wolchok, S. M. Larson, U. Wiesner, M. S. Bradbury, *J. Clin. Invest.* **2011**, *121*, 2768.
[55] M.-Y. Lee, W. H. Kong, H. S. Jung, S. K. Hahn, *RSC Adv.* **2014**, *4*, 19338.
[56] D. Lee, S. Beack, J. Yoo, S.-K. Kim, C. Lee, W. Kwon, S. K. Hahn, C. Kim, *Adv. Funct. Mater.* **2018**, *28*, 1800941.
[57] X. Hao, X. Hu, C. Zhang, S. Chen, Z. Li, X. Yang, H. Liu, G. Jia, D. Liu, K. Ge, X.-J. Liang, J. Zhang, *ACS Nano* **2015**, *9*, 9614.
[58] Y. He, B. Zeng, S. Liang, M. Long, H. Xu, *ACS Appl. Mater. Interfaces* **2017**, *9*, 44402.
[59] Y.-K. Peng, C.-L. Liu, H.-C. Chen, S.-W. Chou, W.-H. Tseng, Y.-J. Tseng, C.-C. Kang, J.-K. Hsiao, P.-T. Chou, *J. Am. Chem. Soc.* **2013**, *135*, 18621.
[60] Y.-K. Peng, Y.-J. Tseng, C.-L. Liu, S.-W. Chou, Y.-W. Chen, S. C. E. Tsang, P.-T. Chou, *Nanoscale* **2015**, *7*, 2676.
[61] K. K. Pohaku Mitchell, A. Liberman, A. C. Kummel, W. C. Trogler, *J. Am. Chem. Soc.* **2012**, *134*, 13997.
[62] L. Yu, Y. Chen, M. Wu, X. Cai, H. Yao, L. Zhang, H. Chen, J. Shi, *J. Am. Chem. Soc.* **2016**, *138*, 9881.
[63] S. Zhang, Z. Chu, C. Yin, C. Zhang, G. Lin, Q. Li, *J. Am. Chem. Soc.* **2013**, *135*, 5709.
[64] S. Zhao, S. Zhang, J. Ma, L. Fan, C. Yin, G. Lin, Q. Li, *Nanoscale* **2015**, *7*, 16389.
[65] a) J. M. Estrela, A. Ortega, E. Obrador, *Cri. Rev. Clin. Lab. Sci.* **2006**, *43*, 143; b) G. K. Balendiran, R. Dabur, D. Fraser, *Cell Biochem. Funct.* **2004**, *22*, 343.
[66] Y. Chen, Q. Meng, M. Wu, S. Wang, P. Xu, H. Chen, Y. Li, L. Zhang, L. Wang, J. Shi, *J. Am. Chem. Soc.* **2014**, *136*, 16326.
[67] a) N. Lu, W. Fan, X. Yi, S. Wang, Z. Wang, R. Tian, O. Jacobson, Y. Liu, B. C. Yung, G. Zhang, Z. Teng, K. Yang, M. Zhang, G. Niu, G. Lu, X. Chen, *ACS Nano* **2018**, *12*, 1580; b) L. Yu, Y. Chen, H. Lin, W. Du, H. Chen, J. Shi, *Biomaterials* **2018**, *161*, 292.
[68] a) J. Della Rocca, R. C. Huxford, E. Comstock-Duggan, W. Lin, *Angew. Chem. Int. Ed.* **2011**, *50*, 10330; b) J. D. Rocca, M. E. Werner, S. A. Kramer, R. C. Huxford-Phillips, R. Sukumar, N. D. Cummings, J. L. Vivero-Escoto, A. Z. Wang, W. Lin, *Nanomedicine* **2015**, *11*, 31.
[69] Y. Fatieiev, J. G. Croissant, K. Julfakyan, L. Deng, D. H. Anjum, A. Gurinov, N. M. Khashab, *Nanoscale* **2015**, *7*, 15046.
[70] J. G. Croissant, Y. Fatieiev, K. Julfakyan, J. Lu, A.-H. Emwas, D. H. Anjum, H. Omar, F. Tamanoi, J. I. Zink, N. M. Khashab, *Chem. Eur. J.* **2016**, *22*, 14806.
[71] L. Zhao, W. Yuan, C. Y. Ang, Q. Qu, Y. Dai, Y. Gao, Z. Luo, J. Wang, H. Chen, M. Li, F. Li, Y. Zhao, *Adv. Funct. Mater.* **2016**, *26*, 3036.
[72] L. Zhao, W. Yuan, H. P. Tham, H. Chen, P. Xing, H. Xiang, X. Yao, X. Qiu, Y. Dai, L. Zhu, F. Li, Y. Zhao, *Small* **2017**, *13*, 1700963.
[73] S. O. Stead, S. J. P. McInnes, S. Kireta, P. D. Rose, S. Jesudason, D. Rojas-Canales, D. Warther, F. Cunin, J.-O. Durand, C. J. Drogemuller, R. P. Carroll, P. T. Coates, N. H. Voelcker, *Biomaterials* **2018**, *155*, 92.
[74] J. Zhang, J. Zhang, W. Li, R. Chen, Z. Zhang, W. Zhang, Y. Tang, X. Chen, G. Liu, C.-S. Lee, *Theranostics* **2017**, *7*, 3007.
[75] a) R. R. Arvizo, S. Bhattacharyya, R. A. Kudgus, K. Giri, R. Bhattacharya, P. Mukherjee, *Chem. Soc. Rev.* **2012**, *41*, 2943; b) R. Hao, R. Xing, Z. Xu, Y. Hou, S. Gao, S. Sun, *Adv. Mater.* **2010**, *22*, 2729.
[76] a) P. Huang, J. Lin, W. Li, P. Rong, Z. Wang, S. Wang, X. Wang, X. Sun, M. Aronova, G. Niu, R. D. Leapman, Z. Nie, X. Chen, *Angew. Chem. Int. Ed.* **2013**, *52*, 13958; b) M. Arruebo, R. Fernández-Pacheco, M. R. Ibarra, J. Santamaría, *Nano Today* **2007**, *2*, 22.
[77] R. Cheheltani, R. M. Ezzibdeh, P. Chhour, K. Pulaparthi, J. Kim, M. Jurcova, J. C. Hsu, C. Blundell, H. I. Litt, V. A. Ferrari, H. R. Allcock, C. M. Sehgal, D. P. Cormode,

Biomaterials **2016**, *102*, 87.
[78] a) W. Zhu, Z. Dong, T. Fu, J. Liu, Q. Chen, Y. Li, R. Zhu, L. Xu, Z. Liu, *Adv. Funct. Mater.* **2016**, *26*, 5490; b) X. Yi, L. Chen, X. Zhong, R. Gao, Y. Qian, F. Wu, G. Song, Z. Chai, Z. Liu, K. Yang, *Nano Res.* **2016**, *9*, 3267.
[79] H. Fan, G. Yan, Z. Zhao, X. Hu, W. Zhang, H. Liu, X. Fu, T. Fu, X.-B. Zhang, W. Tan, *Angew. Chem. Int. Ed.* **2016**, *55*, 5477.
[80] J. Liu, Q. Chen, W. Zhu, X. Yi, Y. Yang, Z. Dong, Z. Liu, *Adv. Funct. Mater.* **2017**, *27*, 1605926.
[81] Y. Chen, D. Ye, M. Wu, H. Chen, L. Zhang, J. Shi, L. Wang, *Adv. Mater.* **2014**, *26*, 7019.
[82] Q. Chen, L. Feng, J. Liu, W. Zhu, Z. Dong, Y. Wu, Z. Liu, *Adv. Mater.* **2016**, *28*, 7129.
[83] G. Yang, L. Xu, Y. Chao, J. Xu, X. Sun, Y. Wu, R. Peng, Z. Liu, *Nat. Commun.* **2017**, *8*, 902.
[84] a) Y. Ueno, H. Futagawa, Y. Takagi, A. Ueno, Y. Mizushima, *J. Controlled Release* **2005**, *103*, 93; b) M. Kester, Y. Heakal, T. Fox, A. Sharma, G. P. Robertson, T. T. Morgan, E. İ. Altinoğlu, A. Tabaković, M. R. Parette, S. M. Rouse, V. Ruiz-Velasco, J. H. Adair, *Nano Lett.* **2008**, *8*, 4116.
[85] Z. Dong, L. Feng, W. Zhu, X. Sun, M. Gao, H. Zhao, Y. Chao, Z. Liu, *Biomaterials* **2016**, *110*, 60.
[86] Z. Dong, L. Feng, Y. Hao, M. Chen, M. Gao, Y. Chao, H. Zhao, W. Zhu, J. Liu, C. Liang, Q. Zhang, Z. Liu, *J. Am. Chem. Soc.* **2018**, *140*, 2165.
[87] L. Xu, G. Tong, Q. Song, C. Zhu, H. Zhang, J. Shi, Z. Zhang, *ACS Nano* **2018**, *12*, 6806.
[88] a) J. Li, Y.-C. Chen, Y.-C. Tseng, S. Mozumdar, L. Huang, *J. Controlled Release* **2010**, *142*, 416; b) J. Li, Y. Yang, L. Huang, *J. Controlled Release* **2012**, *158*, 108.
[89] a) Z. Li, S. L. Wong, *Mater. Sci. Eng. C* **2017**, *70*, 1095; b) A. A. Tedstone, D. J. Lewis, P. O'Brien, *Chem. Mater.* **2016**, *28*, 1965.
[90] M. Zhou, J. Li, S. Liang, A. K. Sood, D. Liang, C. Li, *ACS Nano* **2015**, *9*, 7085.
[91] N. Ma, M.-K. Zhang, X.-S. Wang, L. Zhang, J. Feng, X.-Z. Zhang, *Adv. Funct. Mater.* **2018**, *28*, 1801139.
[92] X.-D. Zhang, J. Zhang, J. Wang, J. Yang, J. Chen, X. Shen, J. Deng, D. Deng, W. Long, Y.-M. Sun, C. Liu, M. Li, *ACS Nano* **2016**, *10*, 4511.
[93] T. Liu, Y. Chao, M. Gao, C. Liang, Q. Chen, G. Song, L. Cheng, Z. Liu, *Nano Res.* **2016**, *9*, 3003.
[94] S. Yan, B. E. Rolfe, B. Zhang, Y. H. Mohammed, W. Gu, Z. P. Xu, *Biomaterials* **2014**, *35*, 9508.
[95] Z. Gu, J. J. Atherton, Z. P. Xu, *Chem. Commun.* **2015**, *51*, 3024.
[96] S. Wang, Y. Wu, R. Guo, Y. Huang, S. Wen, M. Shen, J. Wang, X. Shi, *Langmuir* **2013**, *29*, 5030.
[97] a) V. R. R. Cunha, R. B. de Souza, A. M. C. R. P. da Fonseca Martins, I. H. J. Koh, V. R. L. Constantino, *Sci. Rep.* **2016**, *6*, 30547; b) W. Chen, H. Zuo, T. J. Mahony, B. Zhang, B. Rolfe, Z. P. Xu, *Sci. Rep.* **2017**, *7*, 13367.
[98] W. Chen, H. Zuo, B. Li, C. Duan, B. Rolfe, B. Zhang, T. J. Mahony, Z. P. Xu, *Small* **2018**, *14*, 1704465.
[99] J. Hao, G. Song, T. Liu, X. Yi, K. Yang, L. Cheng, Z. Liu, *Adv. Sci.* **2017**, *4*, 1600160.
[100] L. Cheng, K. Yang, M. Shao, X. Lu, Z. Liu, *Nanomedicine* **2011**, *6*, 1327.
[101] L. Xiong, T. Yang, Y. Yang, C. Xu, F. Li, *Biomaterials* **2010**, *31*, 7078.
[102] S.-t. Yang, W. Guo, Y. Lin, X.-y. Deng, H.-f. Wang, H.-f. Sun, Y.-f. Liu, X. Wang, W. Wang, M. Chen, Y.-p. Huang, Y.-P. Sun, *J. Phys. Chem. C* **2007**, *111*, 17761.
[103] Z. Liu, C. Davis, W. Cai, L. He, X. Chen, H. Dai, *Proc. Natl. Acad. Sci. U.S.A.* **2008**, *105*, 1410.

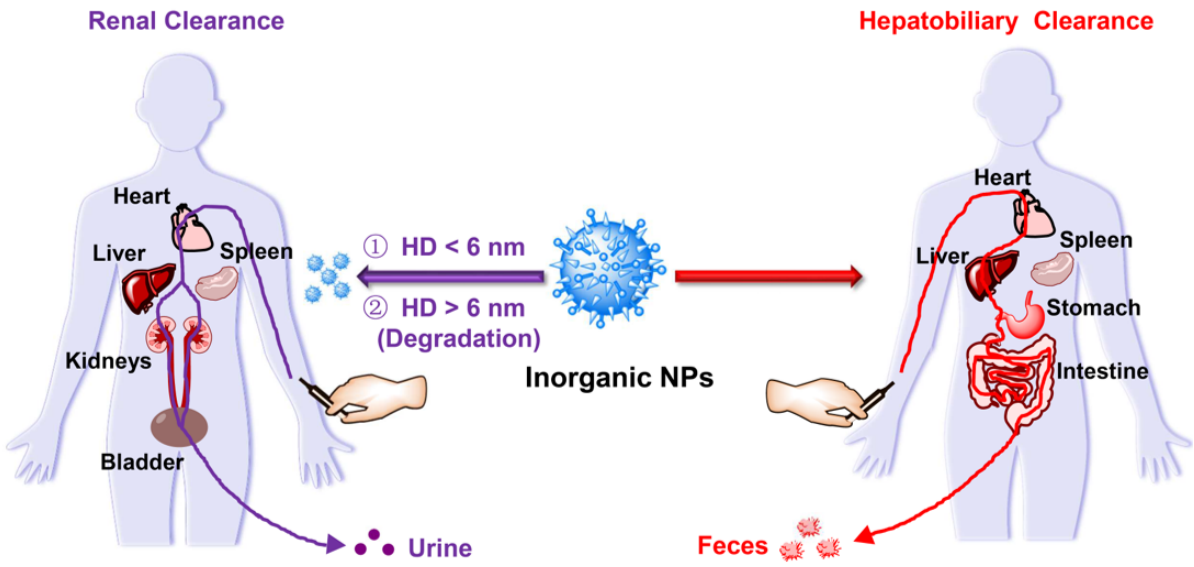

Figure 1. Schematic illustration for the primary metabolic pathway of inorganic nanoparticles in the body. NPs: nanoparticles.

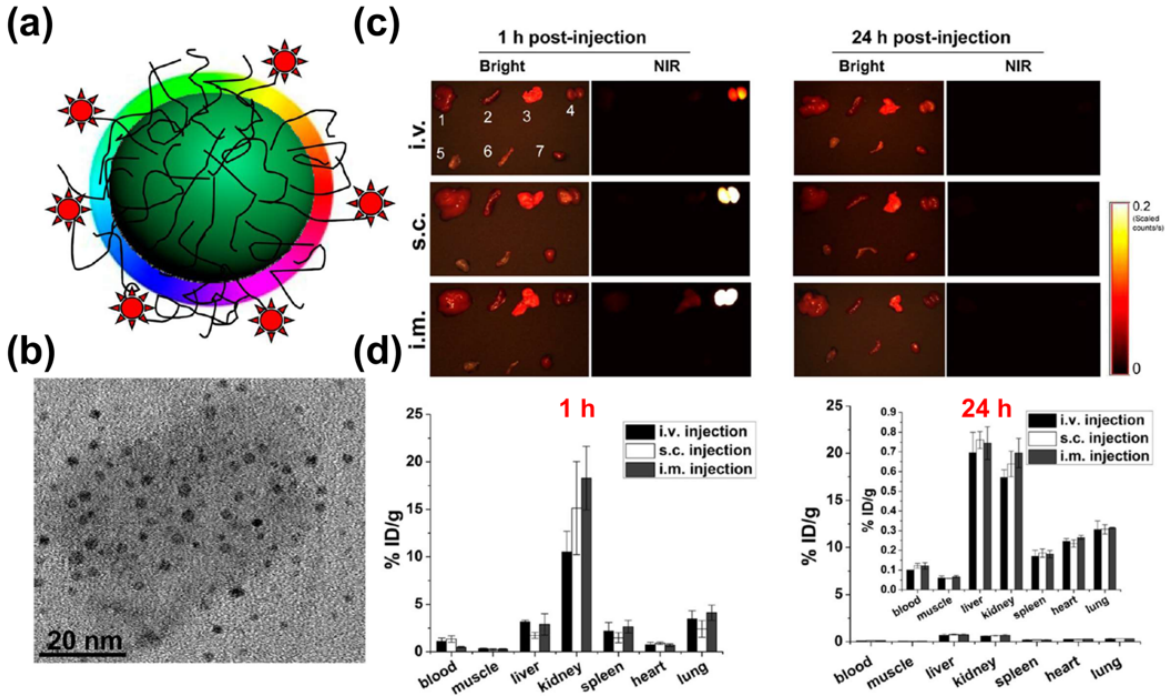

Figure 2. (a) Schematic structure and (b) TEM image of C dots. (c) *Ex vivo* fluorescence imaging of major organs after injection of C dots. The major organs under bright field were 1: liver, 2: spleen, 3: lung, 4: kidneys, 5: muscle, 6: intestine, and 7: heart. (d) Injection dose percentage of major organs after injection of ^{64}Cu-labeled C dots *via* different administrative methods at various time points (1 h and 24 h). Reproduced with permission.[21] Copyright 2013, American Chemical Society.

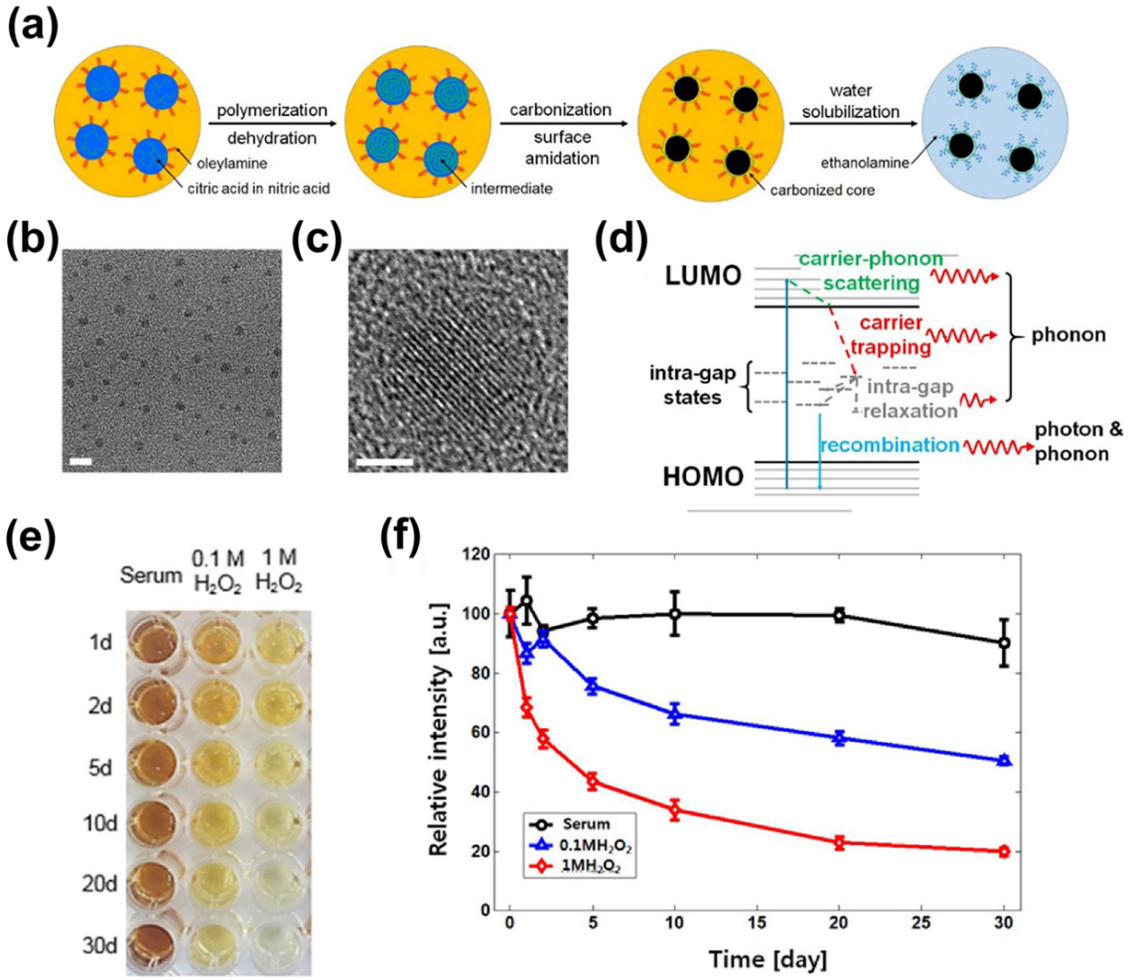

Figure 3. (a) Synthetic process of N-CNDs. (b) TEM image of N-CNDs (scale bar = 5 nm). (c) Magnified TEM image of N-CNDs (scale bar = 2 nm). (d) Description of electronic structure and state of nitrogen-induced intra-gap of N-CNDs. (e,f) Serum biochemistry assay of mice after the injection of N-CNDs. Reproduced with permission.[24] Copyright 2016, Ivyspring International Publisher.

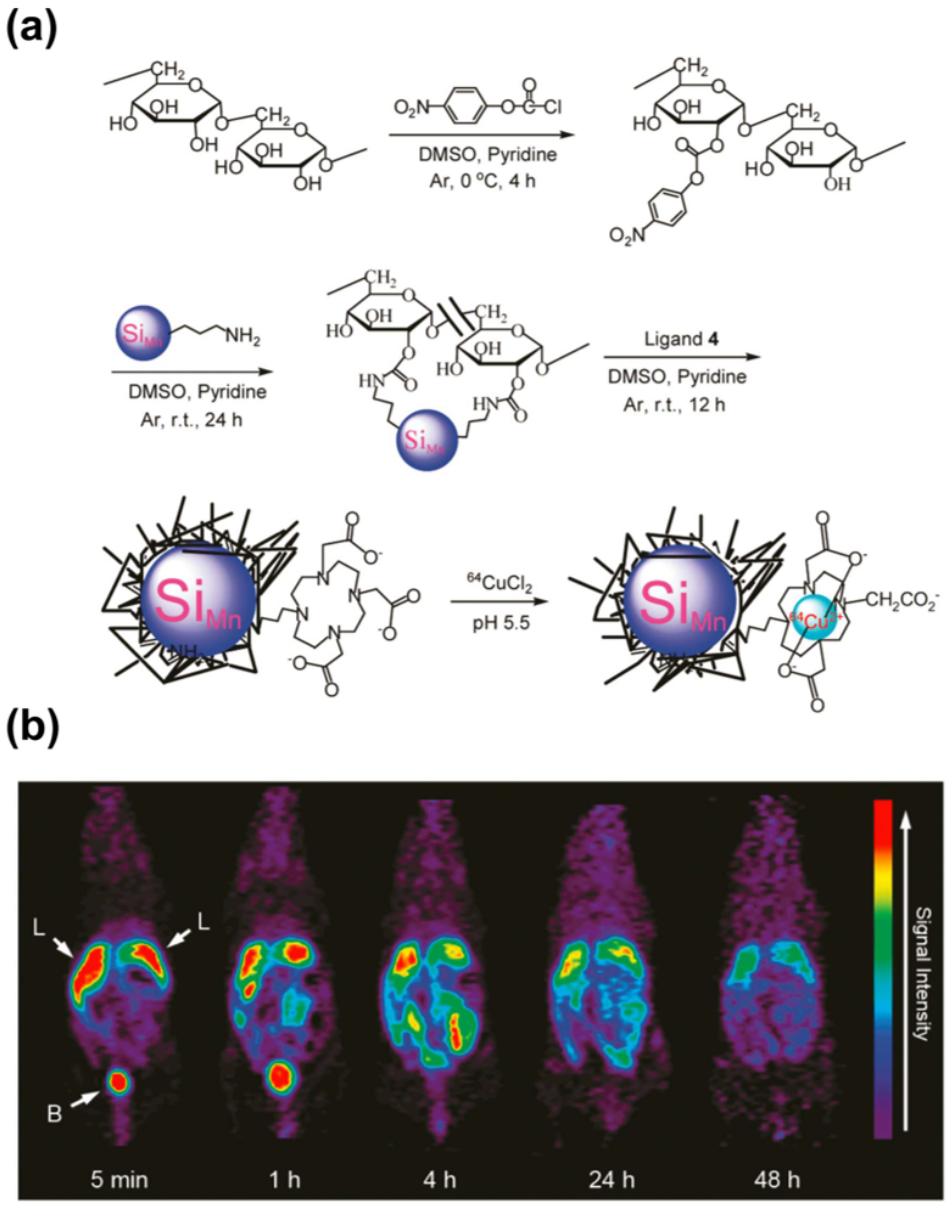

Figure 4. (a) Preparation of ^{64}Cu-DO3A conjugated dextran Si_{Mn} QDs. (b) *In vivo* PET images of mice at different time points (5 min, 1 h, 4 h, 24 h and 48 h) after injecting of ^{64}Cu-DO3A conjugated dextran Si_{Mn} QDs. L: liver, B: bladder. Reproduced with permission.[30] Copyright 2011, American Chemical Society.

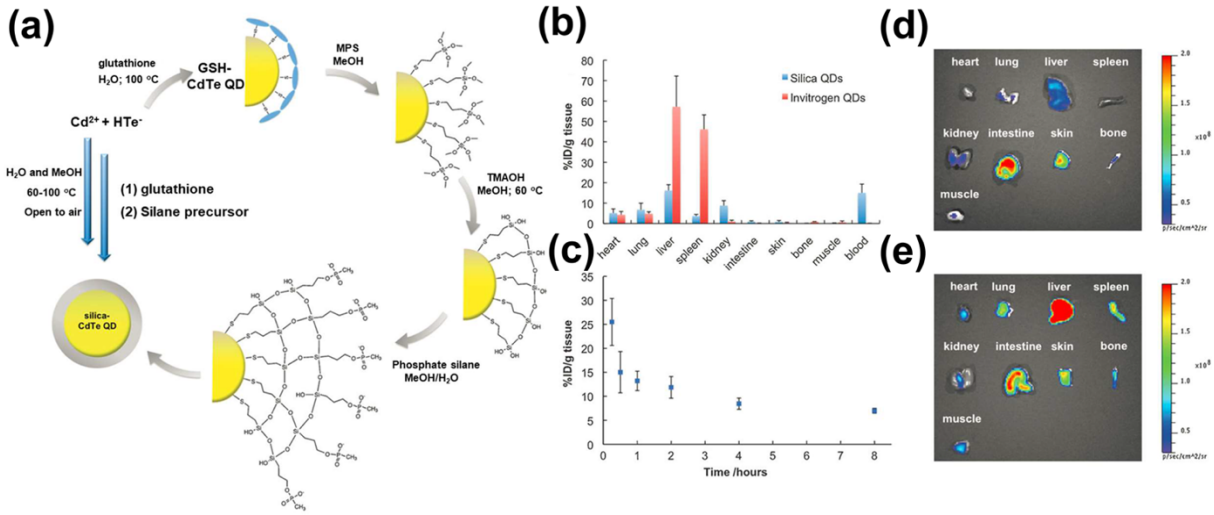

Figure 5. (a) Schematic diagram for the synthesis of silica-coated CdTe QDs. (b) Quantitative analysis for the biodistribution of silica-coated QDs and Invitrogen QDs by inductively coupled plasma atomic emission spectroscopy (ICP-AES). (c) Blood circulation of silica-coated QDs. *In vivo* fluorescence imaging of major organs after i.v. injection of (d) silica-coated QDs and (e) Invitrogen QDs. Reproduced with permission.[34] Copyright 2010, John Wiley and Sons.

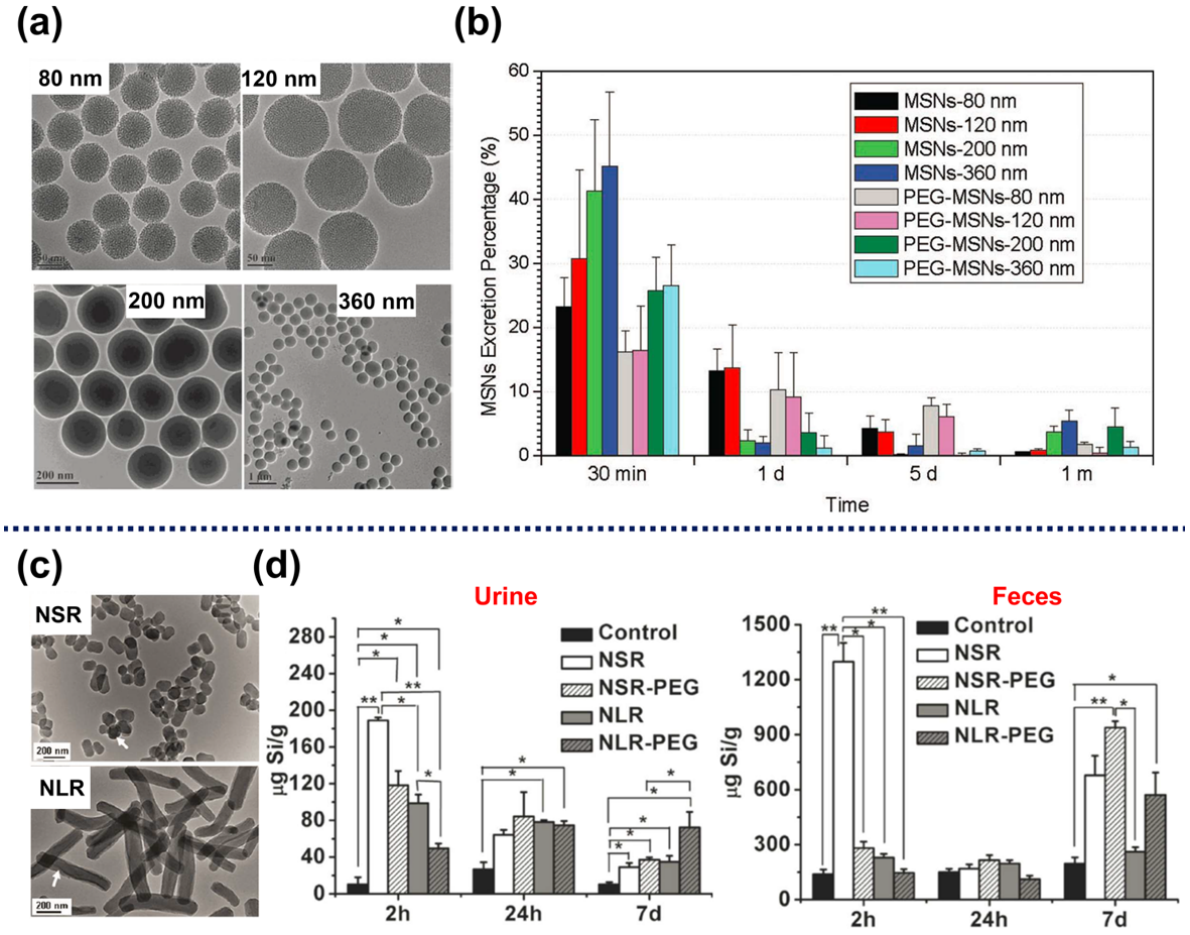

Figure 6. (a) TEM images of PEG-MSNs with different sizes (80, 120, 200 and 360 nm). (b) Excretion percentages of MSNs and PEG-MSNs with different sizes from the urine of mice after i.v. injection. (c) TEM images of fluorescein isothiocyanate (FITC) labelled short rod- and long rod-shaped MSNs (*i.e.*, NSR-FITC and NLR-FITC). (d) Si contents analyzed by ICP-OES in urine and feces at different time points after injection. * and ** indicate statistical significance for Si contents in urine and feces after treating with different shaped and PEGylated MSNs. **p < 0.01, *p < 0.05. (a,b) Reproduced with permission.[41] Copyright 2011, John Wiley and Sons. (c,d) Reproduced with permission.[43] Copyright 2011, American Chemical Society.

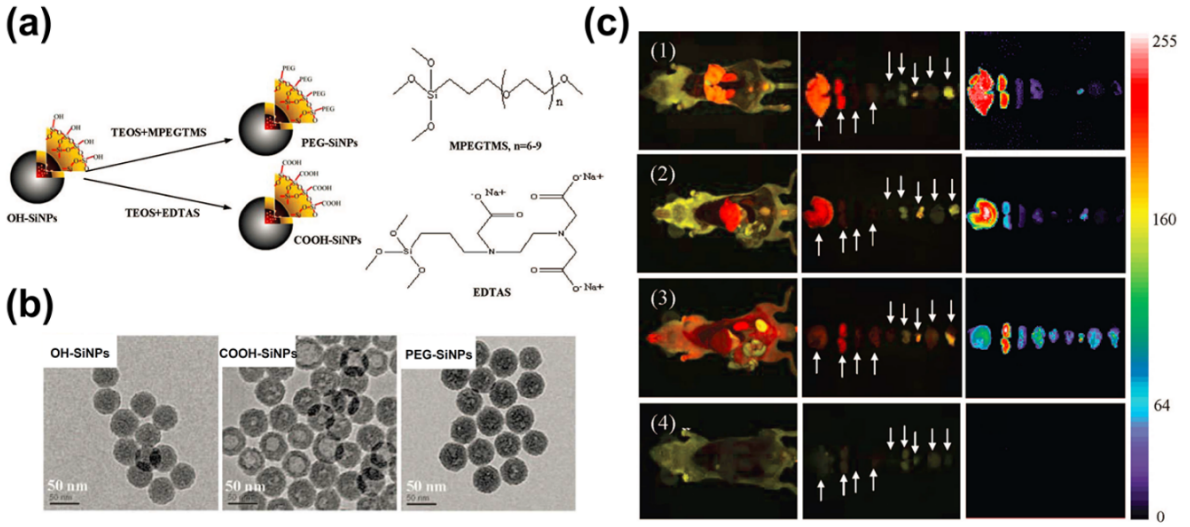

Figure 7. (a) Schematic illustration for the preparation of three types of surface-modified SiNPs. (b) TEM images of three types of surface-modified SiNPs including OH-SiNPs, COOH-SiNPs and PEG-SiNPs. (c) *Ex vivo* imaging of mice after i.v. injection of surface-modified SiNPs along with some organs during necropsy at 4.5 h. (1): OH-SiNPs, (2) COOH-SiNPs, and (3) PEG-SiNPs treated mice, as well as (4) untreated mice. The organs are in the sequence of liver, kidney, spleen, lung, heart, spermary, bladder, brain and muscle. Reproduced with permission.[46] Copyright 2008, American Chemical Society.

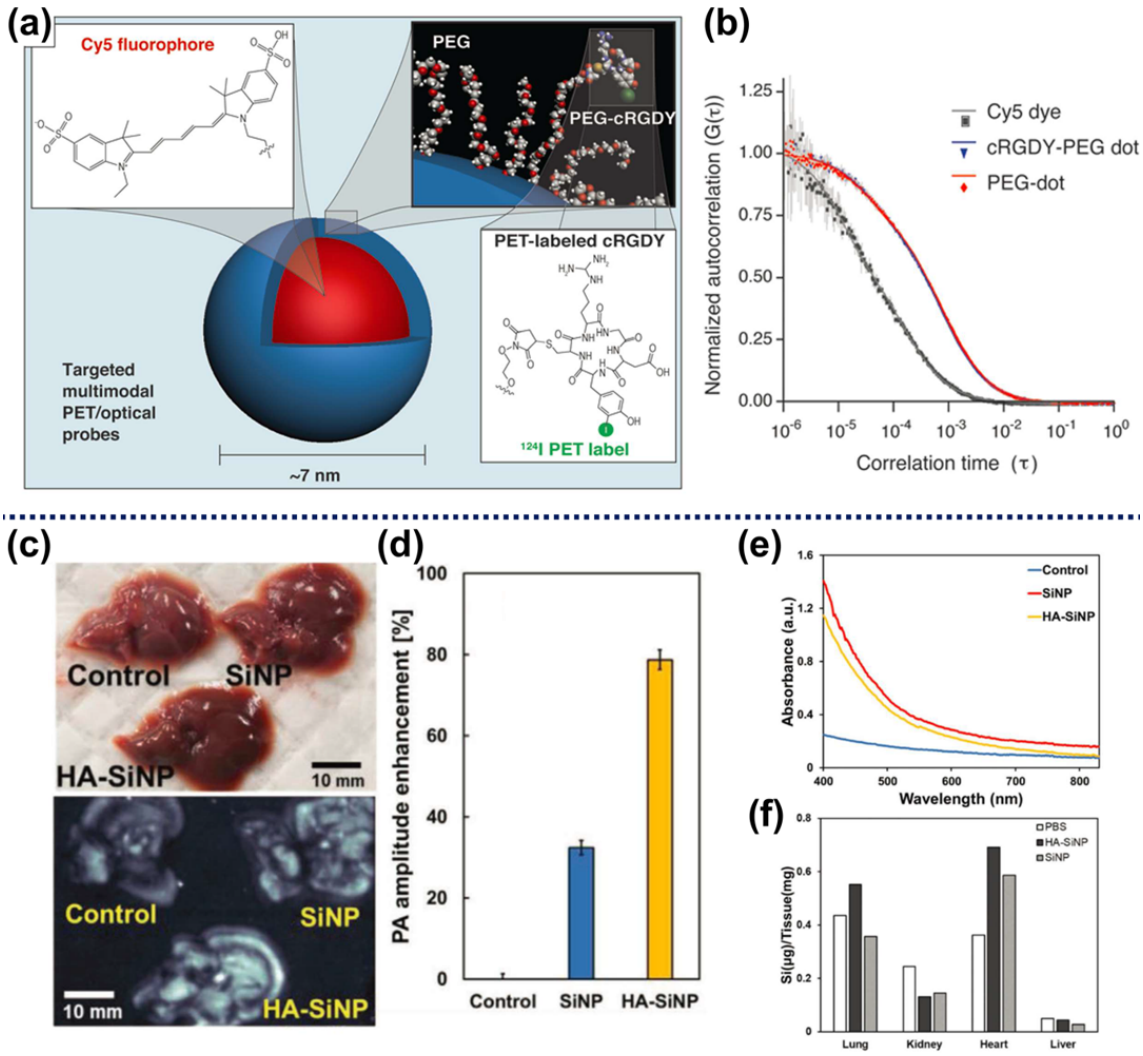

Figure 8. (a) Schematic diagram of ^{124}I-cRGDY-PEG-ylated core-shell silica nanoparticle. (b) Fluorescence correlation spectroscopy (FCS) and single exponential fits for measurements of different samples. (c) Photograph and *ex vivo* PA images of liver after 12 h of SiNP and HA-SiNP injections. (d) *Ex vivo* PA amplitude enhancement in liver after SiNP and HA-SiNP injections. (e) PA spectra of urine after 48 h of SiNP and HA-SiNP injections. (f) Biodistribution of Si element in different organs of mouse after 48 h of SiNP and HA-SiNP injections. (a,b) Reproduced with permission.[54] Copyright 2011, American Society for Clinical Investigation. (c-f) Reproduced with permission.[56] Copyright 2018, John Wiley and Sons.

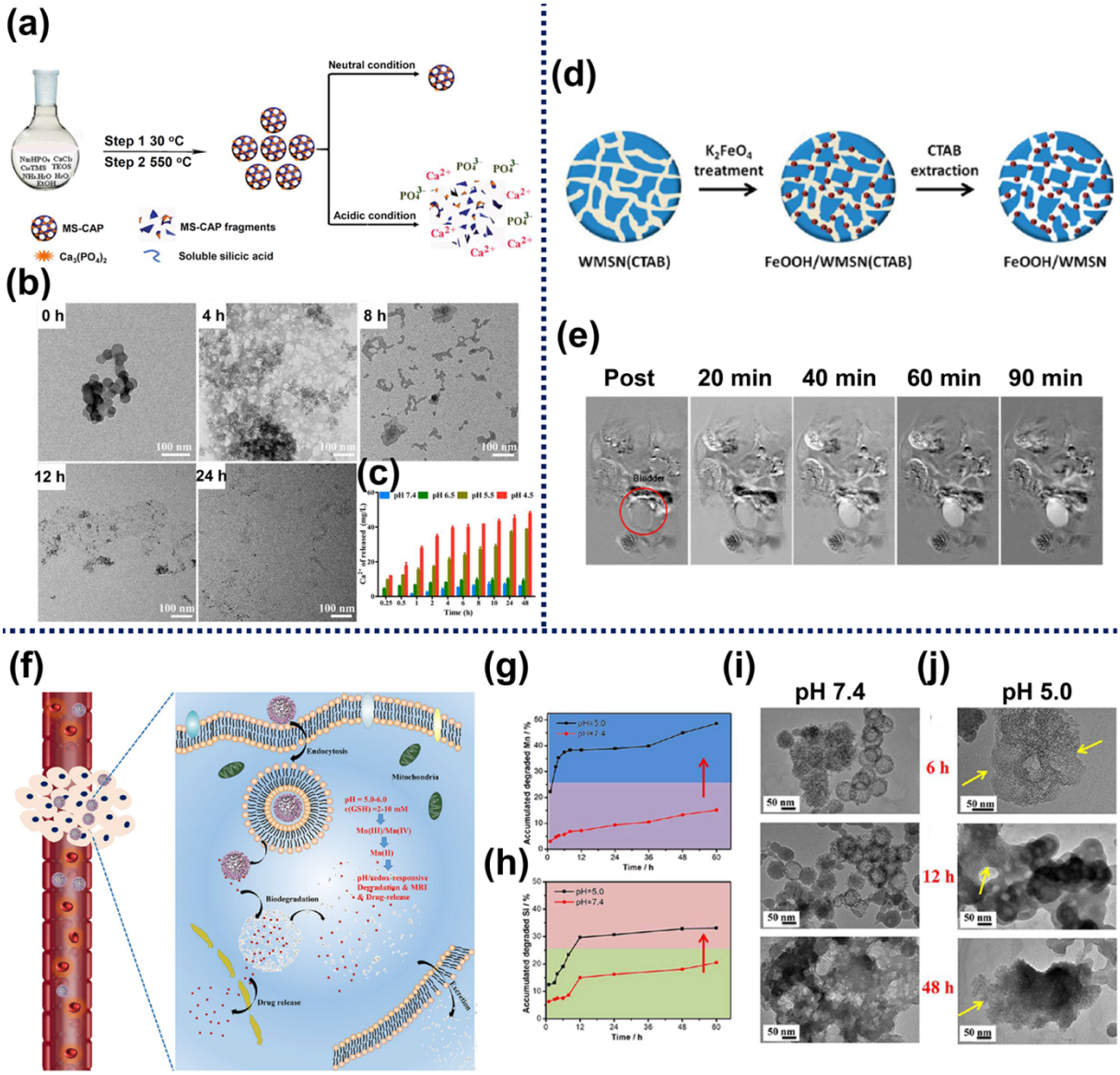

Figure 9. (a) Schematic diagram for the synthesis and degradation of MS-CAP nanoparticles. (b) TEM images of MS-CAP nanoparticles after the degradation under acid environment (pH 4.5) for 0, 4, 8, 12, and 24 h. (c) Release of Ca^{2+} under different pH values (4.5, 5.5, 6.5, and 7.4). (d) Schematic presentation for the synthesis of FeCOOH/WMSN nanoparticles. (e) T1-weighted images of a mouse bladder at various time points (0, 20, 40, 60 and 90 min) after i.v. injection of FeCOOH/WMSN nanoparticles. (f) Schematic illustration of PEG/Mn-HMSNs for pH/redox-responsive degradation and drug delivery. Accumulated degradation of (g) Mn and (h) Si components in SBF at different acidic pH (5.0 and 7.4). TEM images showing the morphological changes of Mn-HMSNs at pH (i) 7.4 and (j) 5.0 for 6, 12 and 48 h. (a-c) Reproduced with permission.[58] Copyright 2017, American Chemical Society. (d,e) Reproduced with permission.[59] Copyright 2013, American Chemical Society. (f-j) Reproduced with permission.[62] Copyright 2016, American Chemical Society.

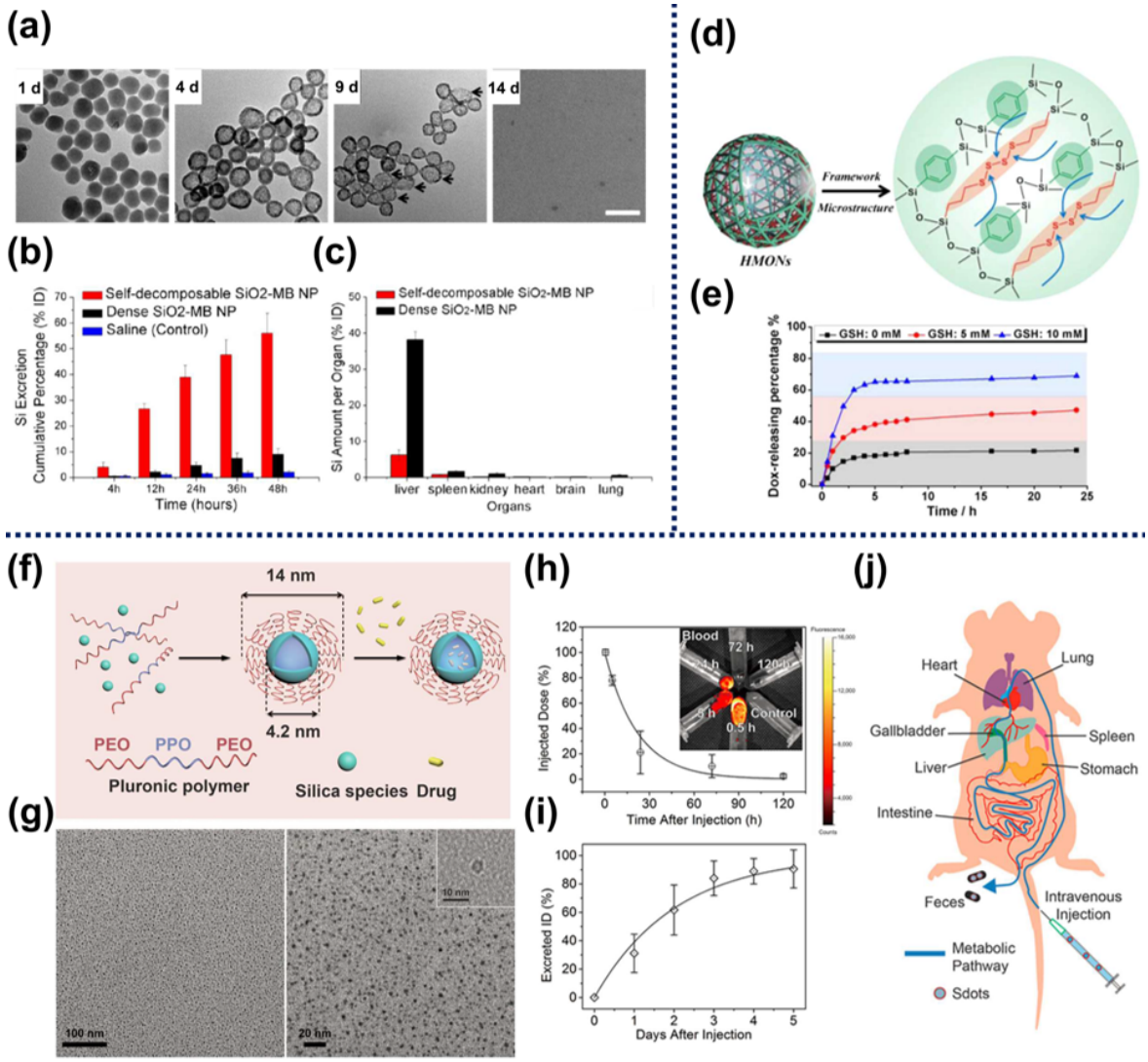

Figure 10. (a) TEM images of the SiO_2-MB (MB = methylene blue) after incubation in water for different days (1, 4, 9 and 14 days). Scale bar: 100 nm. (b) ICP-OES analysis of Si content in the urine of rats at different time points (*i.e.*, 4, 12, 24, 36 and 48 h) after injection of saline, self-decomposable SiO_2-MB, and dense SiO_2-MB. (c) Si content analyzed by ICP-OES in different organs at 48 h after injection of self-decomposable and dense SiO_2-MB. (d) Schematic representation of the compositions in the framework of dual-hybridized HMONs (R1: thiother, R2: phenylene). (e) Percentage amount of drug released at different GSH concentrations (0, 5, and 10 mM). (f) Formation process of Sdots by self-assembly of pluronic triblock copolymer and silica species in aqueous solution. (g) TEM images of Sdots. Inset was a high-resolution image. (h) Blood-circulation time of Sdots measured by ICP-OES. Inset was *ex vivo* imaging of blood samples from mice. (i) Excretion speed of Sdots from mice. (j) Illustration showing how the Sdots were metabolized. (a-c) Reproduced with permission.[63] Copyright 2013, American Chemical Society. (d, e) Reproduced with permission.[66] Copyright 2014, American Chemical Society. (f-j) Reproduced with permission.[71] Copyright 2016, John Wiley and Sons.

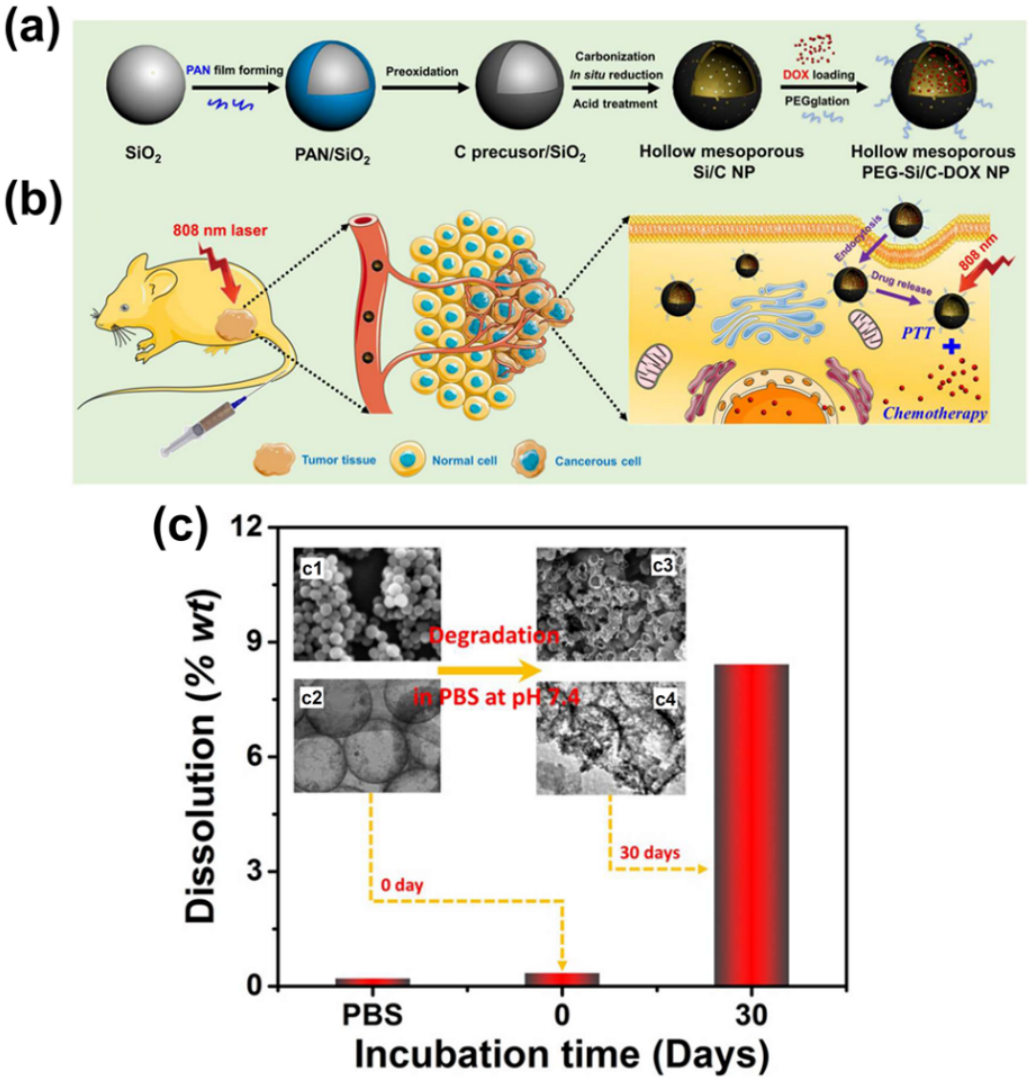

Figure 11. (a) Synthetic process of hollow mesoporous PEG-Si/C-DOX nanoparticles. (b) Application of PEG-Si/C-DOX for PA imaging-guided chemo-thermal therapy. (c) Weight percentage of silicon dissolved in PBS with or without Si/C nanoparticles and incubation for 0 and 30 days at pH 7.4 under continuous shaking. Insets are corresponding SEM (upper) and TEM (lower) images of Si/C nanoparticles (c1,c2) before and (c3,c4) after incubation in PBS for one month. Reproduced with permission.[74] Copyright 2017, Ivyspring International Publisher.

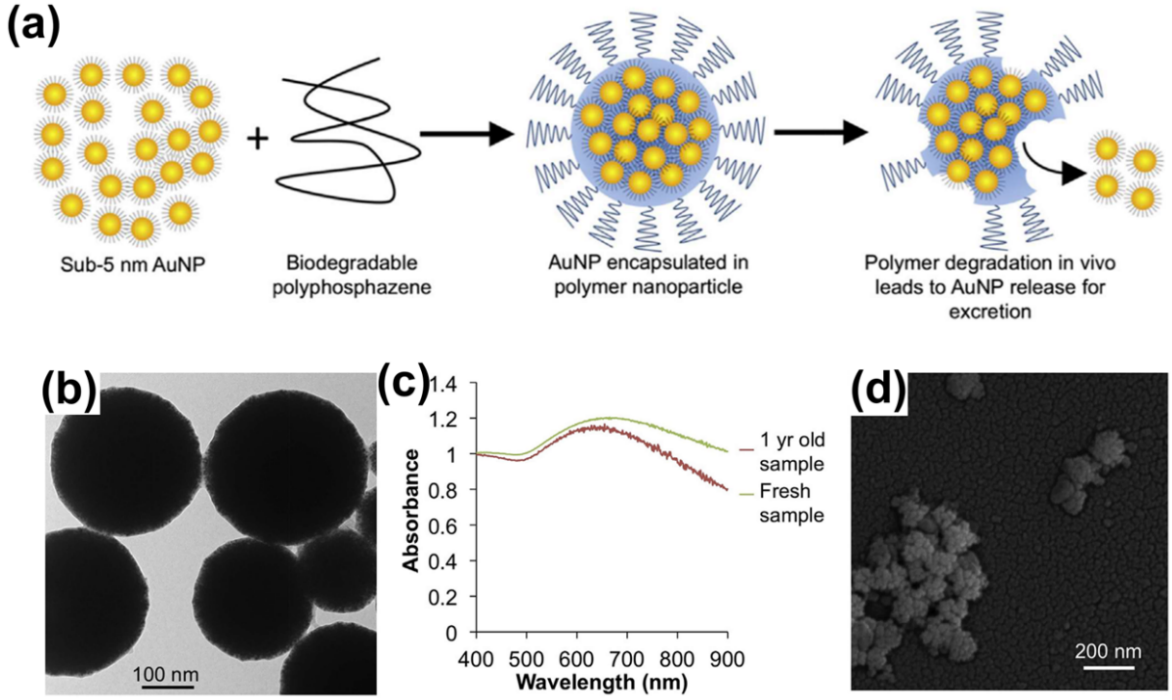

Figure 12. (a) Schematic illustration for the synthesis of biodegradable gold nanoparticles (Au-PCPP). (b) TEM image of Au-PCPP after the preparation for 6 months. (c) UV-vis spectra of freshly synthesized and one-year old Au-PCPP nanoparticles. (d) SEM image of Au-PCPP after one-week incubation in 10 % serum. Reproduced with permission.[77] Copyright 2016, Elsevier.

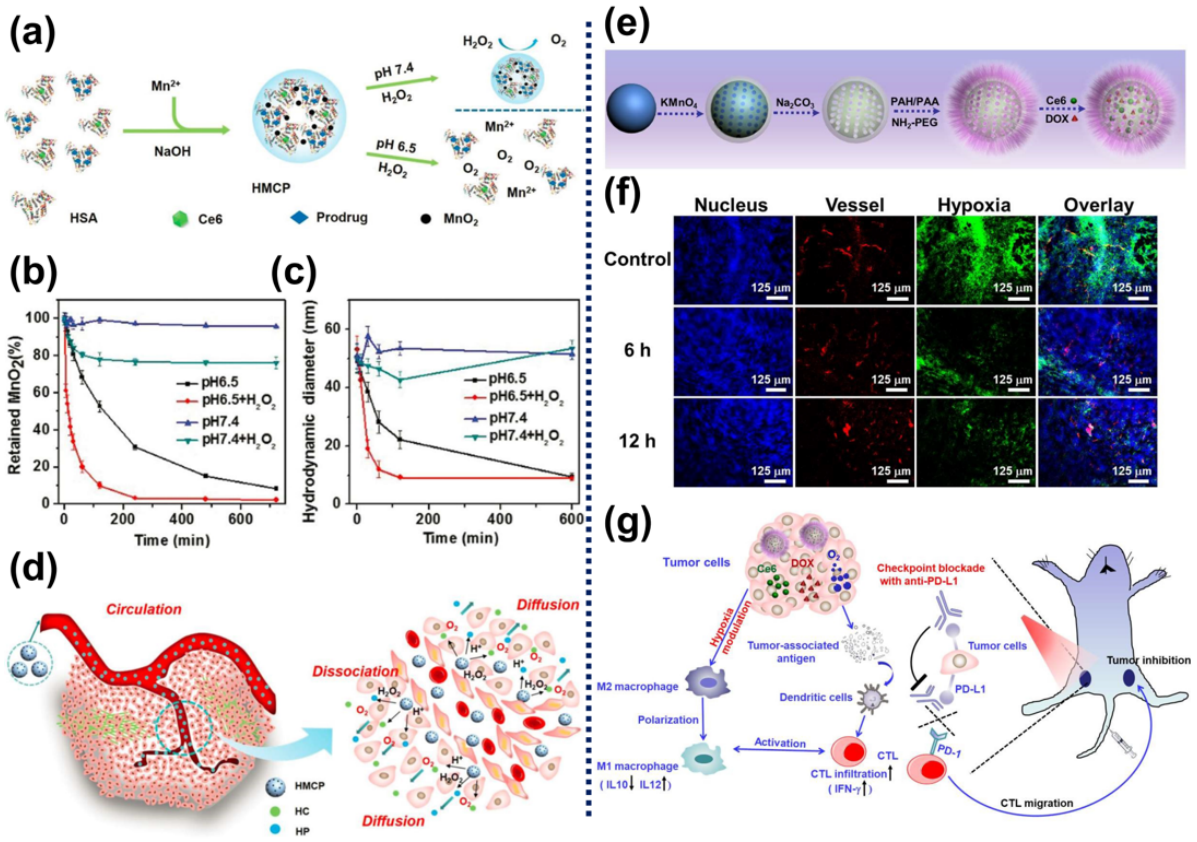

Figure 13. (a) Schematic illustration for the preparation of HMCP nanoparticles and their degradability at different pH conditions (7.4 and 6.5) in the presence of H_2O_2. Degradation of HMCP incubated in different pH values (6.5 and 7.4) with or without H_2O_2 monitored by (b) UV-vis-NIR and (c) DLS in terms of HD with respect to time. (d) Schematic illustration for the decomposition of HMCP in tumor microenvironment to permit interstitial penetration of therapeutic agents (*i.e.*, HSA-Ce6 (HC) and HSA-Pt(IV) (HP)). (e) Illustration for the synthetic procedure of PEG modified hollow MnO_2 and subsequent drug loading. (f) Immunofluorescence images of tumor sections excised from untreated mice and mice that were euthanized 6 and 12 h after i.v. injection of PEG modified hollow MnO_2 loaded with drugs. (g) Proposed mechanism of anti-tumor immune responses of PEG modified hollow MnO_2 loaded with drugs by combining with anti-PD-L1 therapy. (a-d) Reproduced with permission.[82] Copyright 2016, John Wiley and Sons. (e-g) Reproduced with permission.[83] Copyright 2017, Nature Publishing Group.

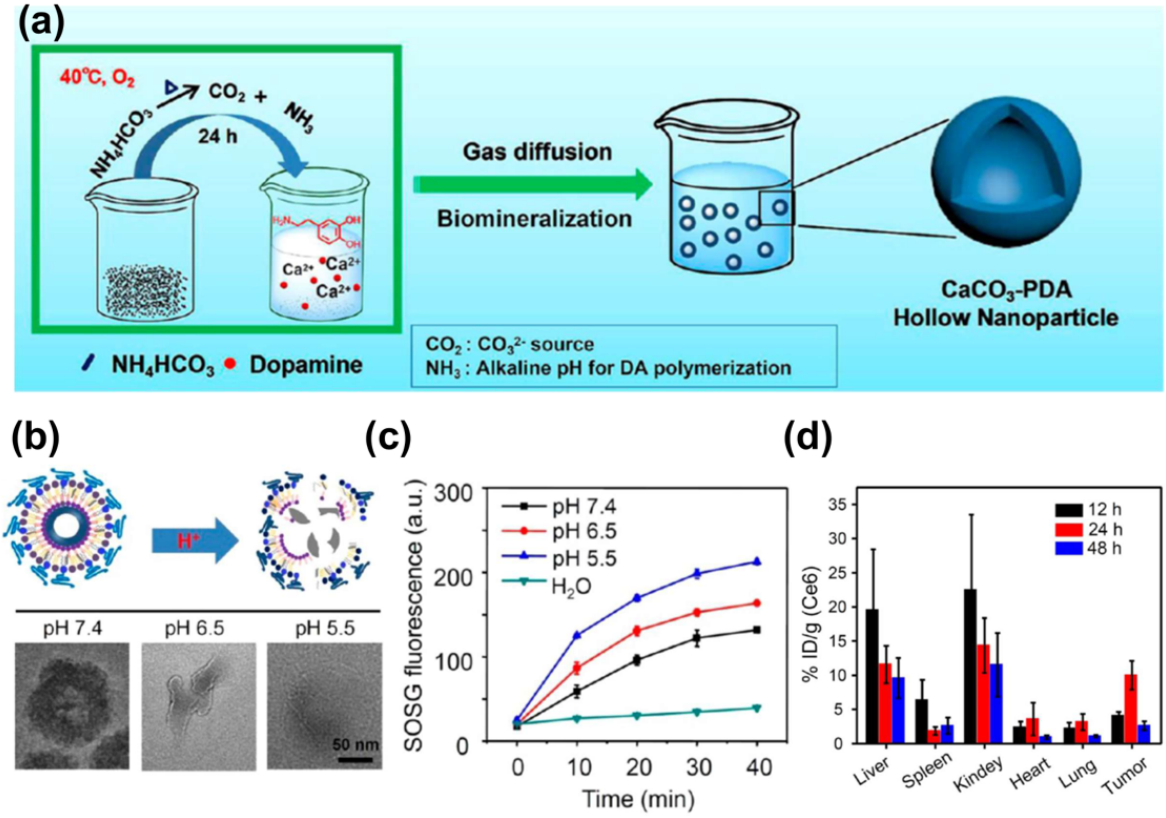

Figure 14. (a) Illustration for the preparation of $CaCO_3$-PDA-PEG hollow nanoparticles. (b) Schematic illustration for the acid-induce degradation of $CaCO_3$-PDA-PEG and corresponding TEM images after incubation in different pH solutions (5.5, 6.5 and 7.4) for 2 h. (c) Singlet oxygen production of Ce6@$CaCO_3$-PDA-PEG monitored over 40 min after being dispersed in different pH conditions. (d) Biodistribution of Ce6@$CaCO_3$-PDA-PEG at different time intervals (12, 24 and 48 h) after i.v. injection, as measured by Ce6 fluorescence. Reproduced with permission.[86] Copyright 2018, American Chemical Society.

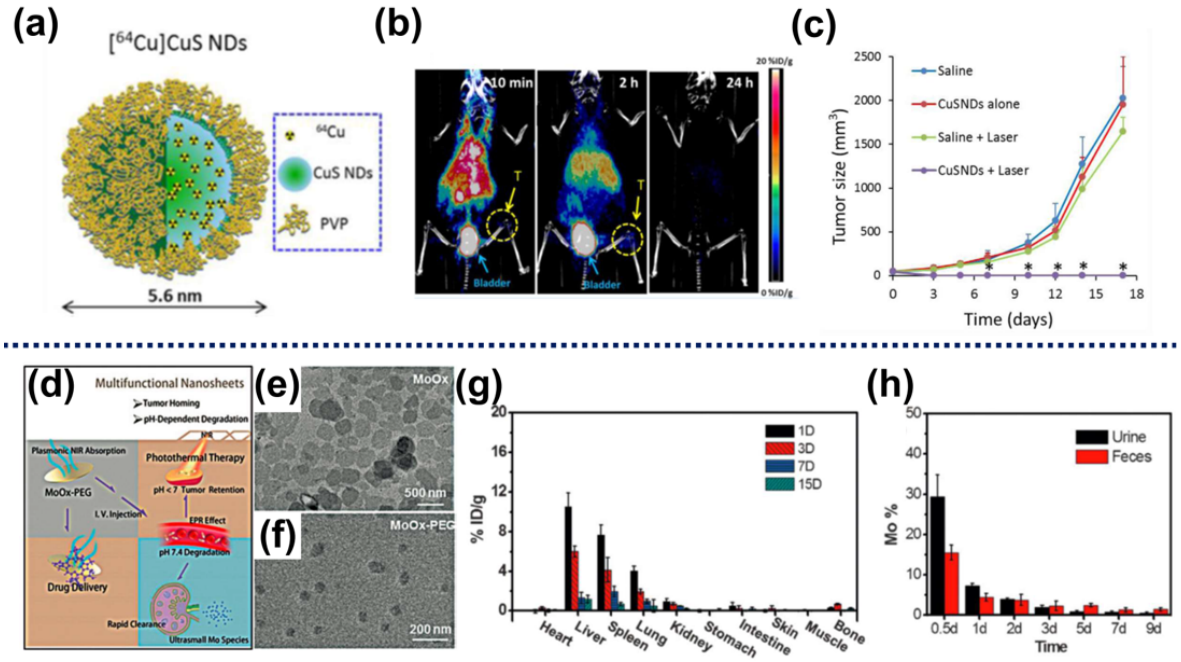

Figure 15. (a) Designed structure of [^{64}Cu]CuS NDs. (b) Overlap of PET and computed tomography images taken at various time points (10 min, 2 h and 24 h) after i.v. injection of [^{64}Cu]CuS NDs into mice bearing 4T1 breast tumor. (c) Tumor growth curves of various groups after different treatments indicated. (d) Process of MoOx-PEG nanosheets for cancer therapy, degradation and excretion. TEM images of (e) as-prepared MoOx and (f) MoOx-PEG. (g) Time-dependent biodistribution of Mo element in mice after i.v. injection of MoOx-PEG. (h) Mo contents in various excretion products including urine and feces obtained at different time points post injected with MoOx-PEG. (a-c) Reproduced with permission.[90] Copyright 2015, American Chemical Society. (d-h) Reproduced with permission.[11] Copyright 2016, John Wiley and Sons.

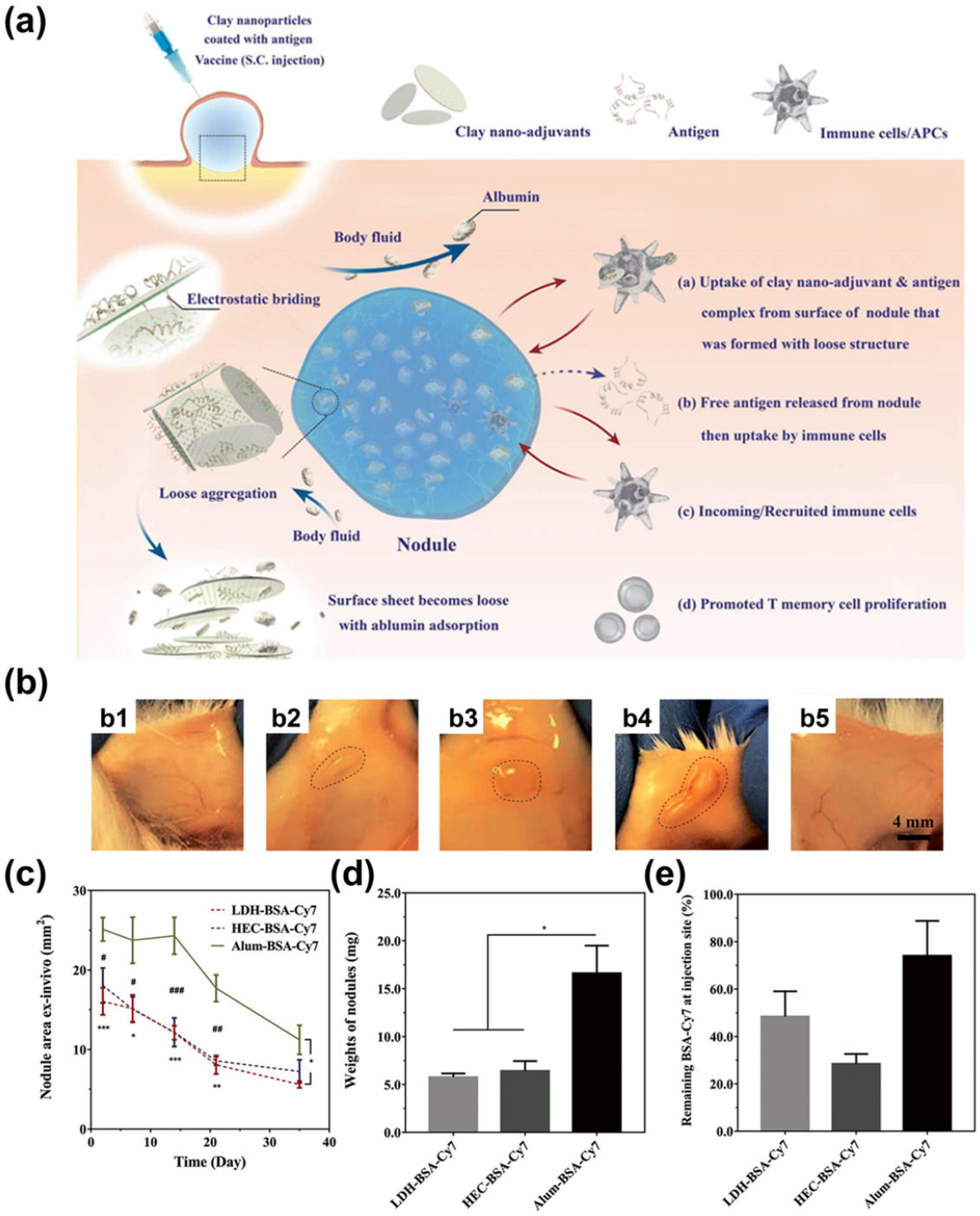

Figure 16. (a) Antigen loaded clay nanoadjuvant forming a loose structure of the nodule at the injection site. (b) Corresponding optical images of nodules formed at the injection site after 35 days. b1: BSA-Cy7, b2: LDH-BSA-Cy7, b3: HEC-BSA-Cy7, b4: Alum-BSA-Cy7, and b5: QuilA-BSA-Cy7. (c) Assessed nodule area from three vaccine groups at different times. "*" and "#" represent significant differences between the three groups. (d) Weights of the nodules obtained from the three groups. (e) Relative remaining amount of BSA-Cy7 in the formed nodules. Reproduced with permission.[98] Copyright 2018, John Wiley and Sons.

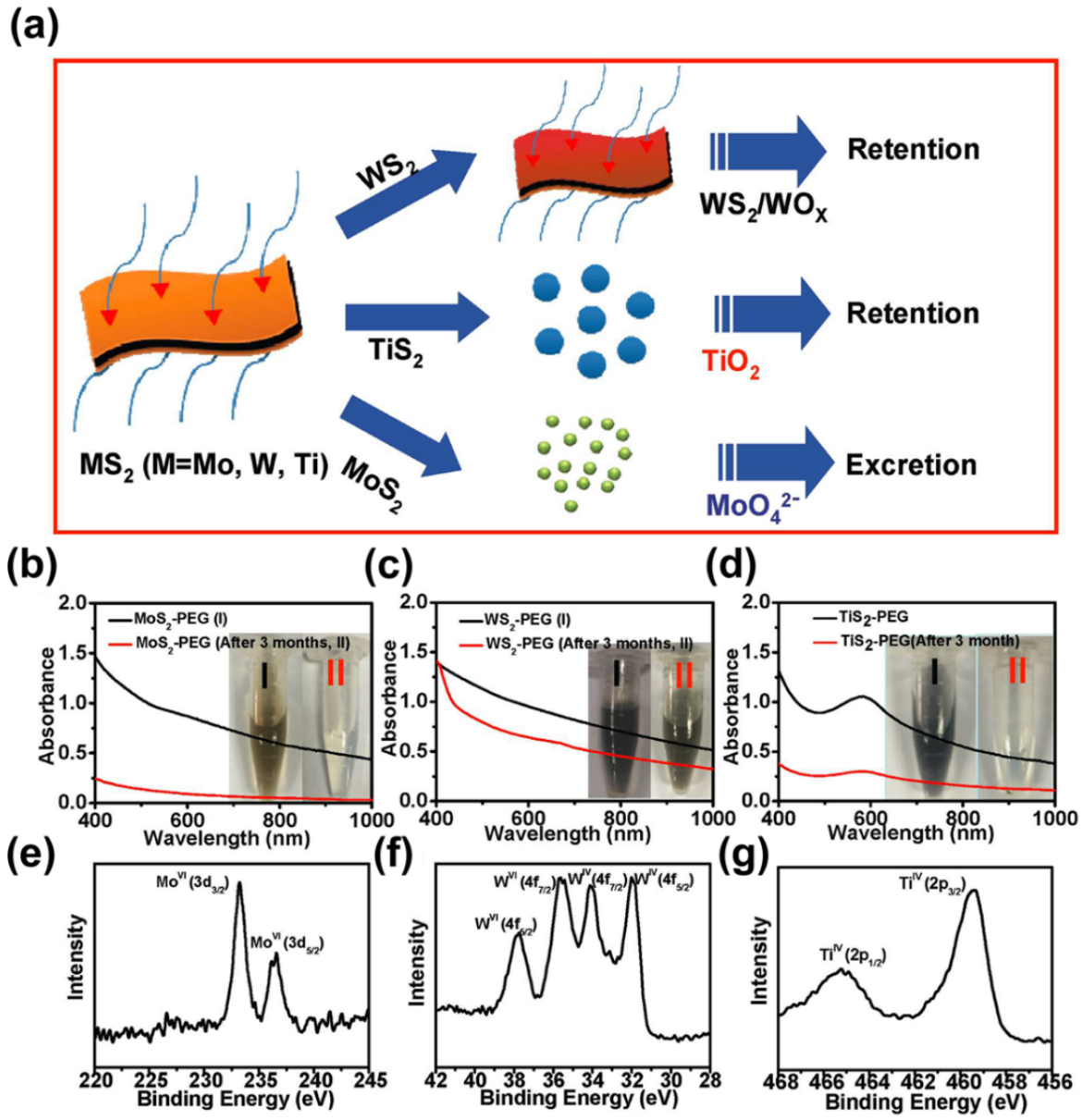

Figure 17. (a) Schematic illustration showing different clearance pathways of MS_2-PEG nanosheets (M: Mo, W, and Ti). (b-d) UV-vis-NIR spectra of MS_2-PEG (I) before and (Ⅱ) after incubation in PBS for three months. (b) MoS_2-PEG, (c) WS_2-PEG, and (d) TiS_2-PEG. Insets show corresponding photos of MS_2-PEG nanosheets (I) before and (Ⅱ) after incubation in PBS for three months. XPS spectra of (e) Mo^{VI+}, (f) W^{VI+} and W^{IV+} after oxidation, and (g) Ti^{IV} of TiO_2 nanoparticles from TiS_2-PEG after incubation in PBS for three months. Reproduced with permission.[99] Copyright 2017, John Wiley and Sons.

TOC Figure:

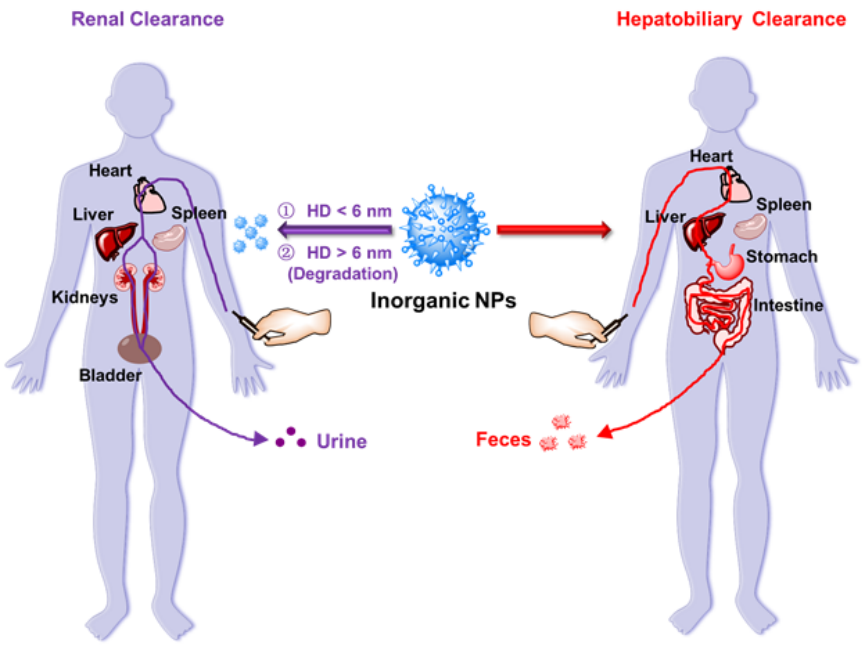

Inorganic nanoparticles with variable compositions possess distinct physical and chemical properties and versatile morphologies and sizes, providing unprecedented opportunities for novel biomedical technologies. This review summarizes various factors that greatly influence the degradability and clearance of different inorganic nanoparticles, aiming to present potential solutions to long-term challenges toward clinical translation.

Guangbao Yang received his Ph.D. degree in 2017 from Soochow University under the guidance of Professor Zhuang Liu. He is now working with Professor Yanli Zhao as a research fellow at Nanyang Technological University. His research is focused on the design and synthesis of multifunctional nanostructures for imaging-guided cancer therapy and tumor microenvironment modulation.

Yanli Zhao is currently a Professor at Nanyang Technological University. He received his B.Sc. degree in chemistry from Nankai University and his Ph.D. degree in physical chemistry there under the supervision of Professor Yu Liu. He was a postdoctoral scholar with Professor Sir Fraser Stoddart at University of California Los Angeles and subsequently at Northwestern University. He also conducted his postdoctoral research with Professor Jeffrey Zink at University of California Los Angeles. His current research focuses on integrated nanoparticles for theranostics, and porous materials for gas storage and catalysis.